

CONTENT

Vol. 10. No. 2-2024

Albert Waal

ALGORITHM AND INSTRUCTIONS FOR PRACTICAL
USE IN THE METHODOLOGY OF COEXISTENCE
OF TELEVISION, FM AND DIGITAL BROADCASTING
IN DAB AND DRM+ STANDARDS

2

Bayram Ibrahimov, Oleg Varlamov

EFFICIENCY ANALYSIS OF SWITCHING
CONVERTER-MODULATOR

12

Mamedov Shamsi Elshan ogly,

Rahimov Elshan Rasif ogly

INFORMATION MODEL OF VEHICLE
TELEMATICS DATA CLUSTER COLLECTION
USING UAV

21

Denis Chicherov

ANALYSIS OF METHODS TO INCREASE QOE
PARAMETERS FOR VIDEO STREAMING
SERVICES

28

Ngok Nuen Tan

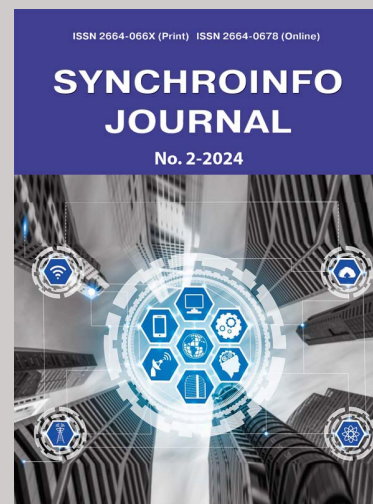
PEAK-TO-AVERAGE POWER RATIO OF
SPECTRALLY EFFICIENT FDM SIGNALS

37

Liu Wenkui

NONCOHERENT DATA TRANSFER BY
USING ORTHOGONAL NOISE SIGNALS

44



Published bi-monthly since 2015

ISSN 2664-0678 (Online)

ISSN 2664-066X (Print)

Publisher

Institute of Radio and Information
Systems (IRIS), Vienna, Austria

Deputy Editor in Chief

Albert Waal

*Dr.-Ing., RF Mondial GmbH,
Hannover, Germany*

Editorial board

Corbett Rowell

Doctor of Science, Rohde & Schwarz, Munich, Germany

Julius Golovatchev

PhD, INCOTELOGY GmbH, Pulheim, Germany

Oleg V. Varlamov

Doctor of Science, IRIS Association, Vienna, Austria

Svetlana S. Dymkova

PhD, IRIS Association, Vienna, Austria

Michael J. Sharpe

*PhD, ETSI/SPR Director Committee Support Centre,
European Telecommunications Standards Institute (ETSI),
Nice Area, France*

Andrey V. Grebennikov

Ph.D., Sumitomo Electric Europe, Elstree, United Kingdom

Eric F. Dulkeith

*Doctor of Science, Senior Executive, Detecon Inc.,
San Francisco, USA*

Marcelo S. Alencar

*Doctor of Science, Federal University of Campina Grande,
Brazil*

German Castellanos-Dominguez

Ph.D., National University of Colombia, Manizales, Colombia

Ali H. Harmouch

*Doctor of Science, University of Business and Technology,
Jeddah, Saudi Arabia*

Valery O. Tikhvinskiy

*Doctor of Science, International Information Technology
University, Almaty, Kazakhstan*

Bayram Ibrahimov

*Doctor of Science, Azerbaijan Technical University, Baku,
Azerbaijan*

Kristina Knox

*Doctor of Philosophy, PhD at The University of Queensland,
Australia*

Anastasia Mozhaeva

*Doctoral Candidate (Computer Vision) The University of
Waikato, Hamilton, New Zealand*

Boudal Niang

*Doctor of Philosophy, Multinational Graduate School of
Telecommunications, Dakar, Senegal*

Address:

*1010 Wien, Austria, Ebendorferstrasse 10/6b
media-publisher.eu/synchroinfo-journal*

© Institute of Radio and Information Systems (IRIS), 2024

ALGORITHM AND INSTRUCTIONS FOR PRACTICAL USE IN THE METHODOLOGY OF COEXISTENCE OF TELEVISION, FM AND DIGITAL BROADCASTING IN DAB AND DRM+ STANDARDS

Albert Waal ¹

¹ RF Mondial GmbH, Hannover, Germany

ABSTRACT

The parameters of the network model are determined on the basis of data contained in the database on frequency assignments of a radio frequency service organization or radio frequency application materials for obtaining an EMC examination conclusion submitted to a radio frequency service organization to obtain permission to use frequency blocks / radio frequency channels for the declared radio broadcasting stations. The problem of sharing the spectrum in the VHF band by terrestrial digital television broadcasting services (DVB-T standard, etc.), analogue television broadcasting, analogue FM audio broadcasting, digital audio broadcasting DAB/DAB+, DRM+ and RAVIS and the conditions for their coexistence are considered. The most common cases of the developed methodology application can be the following options for calculating EMC and conditions for using electronic distribution systems for television and radio broadcasting: Calculation of reference service area of the protected service; Calculation of EMC between existing and planned for use service and declared service; Calculation of service area of the proposed distribution zone.

DOI: [10.36724/2664-066X-2024-10-2-2-11](https://doi.org/10.36724/2664-066X-2024-10-2-2-11)

Received: 12.03.2024

Accepted: 07.04.2024

Citation: Albrt Waal, "Algorithm and instructions for practical use in the methodology of coexistence of television, FM and digital broadcasting in DAB and DRM+ standards," *Synchroinfo Journal* **2024**, vol. 10, no. 2, pp. 2-11

Licensee IRIS, Vienna, Austria.

This article is an open access article distributed under the terms and conditions of the Creative Commons Attribution (CC BY) license (<https://creativecommons.org/licenses/by/4.0/>).



Copyright: © 2024 by the authors.

KEYWORDS: *calculation methodology, coexistence, digital broadcasting, DAB, DRM+, FM broadcasting, television broadcasting, EMC.*

1 Introduction

Despite the widespread introduction of terrestrial digital television broadcasting (DVB-T standard and others) around the world [1-3], analogue television broadcasting [4,5] continues in a number of countries. In some cases, it is carried out in the VHF range. In the same range, analogue FM audio broadcasting [6-8] continues to be carried out, and various types of digital audio broadcasting [9-11], such as DAB/DAB+, DRM+ [12-14] and RAVIS, are being introduced. For this reason, it is necessary to consider the conditions for sharing the spectrum to ensure the coexistence of these types of broadcasting [15-17], which is especially important for the border areas of countries with different rates of digitalization.

Article [18] examines various scenarios for how all of these broadcast services can work together and defines the criteria for ensuring electromagnetic compatibility (EMC). Compatibility criteria and calculation algorithm are considered.

The most common cases of the developed methodology application can be the following options for calculating EMC and conditions for using electronic distribution systems for television and radio broadcasting:

1. Calculation of reference service area of the protected service.
2. Calculation of EMC between existing and planned for use service and declared service.
3. Calculation of service area of the proposed distribution zone.

2 Algorithm for calculating the reference service area of an existing or planned distribution network

The algorithm for calculating reference service area of an existing or planned distribution network contains the following steps:

1. Selecting an existing or planned radio electronics system from the database – Interference receptor.
2. Formation of an array of existing or planned for use services – sources of interference ($n = 1...N$). The selection is carried out from the database using frequency-territorial criteria.
3. Formation of control points ($j = 1...J$). Control points correspond to the locations where radio distribution zones receive television and radio broadcasts and are located within the coverage area of the current or planned distribution zone.

Calculations are carried out within the coverage area (ideal zone) of the protected service, determined in accordance with the minimum used field strength of the service for television and radio broadcasting.

4. Calculation of the useful field strength (E_{us}) of current or planned radio electronics – interference receptor at the j -th control point (1).

$$E_{us} = E(50, 50) + \Delta P, \text{ dB}(\mu\text{V/m}) \quad (1)$$

where $E(50, 50)$ – field strength determined for a reference transmitter with Equivalent Isotropically Radiated Power EIRP =30 dBW, 50% of locations and 50% of reception time, for a representative height, dB($\mu\text{V/m}$); ΔP – correction factor for the effective radiated power relative to the reference transmitter with EIRP =30 dBW.

The effective radiated power is defined as:

$$P = 10 \lg(\text{PTx}_{\text{Tv}}) + \text{GTx}_{\text{Tv}}, \text{ dB(kW)} \quad (2)$$

where PTx_{Tv} – transmitter power, kW; GTx_{Tv} – gain of the transmitting antenna (corrected in accordance with the azimuthal direction to a given design point), dBd.

To more accurately predict the level of field strength, it is desirable to have information about the ground cover (obstacles, building density, terrain) along the route. It is convenient to store obstacle categories in an additional data array for consistency with profile height data.

5. Calculation of the interfering field strength of the n -th operating or planned for use source of interference at the j -th control point (3-5).

$$E_{iT} = E(50, t) + \Delta P + PRT + \Delta A, \text{ dB}(\mu\text{V/m}) \quad (3)$$

$$E_{iC} = E(50, 50) + \Delta P + PRC + \Delta A, \text{ dB}(\mu\text{V/m}) \quad (4)$$

where $E(50, t)$ – field strength determined for a reference transmitter with EIRP=30 dBW, 50% of locations and $t\%$ of reception time, dB($\mu\text{V/m}$); ΔP – correction factor for the effective radiated power relative to the reference transmitter with EIRP=30 dBW, dB; PRT – protection ratio for tropospheric interference, dB; PRC – protection ratio for constant interference, dB; ΔA – correction taking into account the spatial and polarization noise immunity of the receiving antenna (applies only to fixed reception), dB.

$$E_{fi} = E(50, 1) + \Delta P + PR + \Delta A + OLC, \text{ dB}(\mu\text{V/m}) \quad (5)$$

where $E(50, 1)$ – field strength determined for a reference transmitter with EIRP=30 dBW, 50% of locations and 1% of reception time, dB($\mu\text{V/m}$); ΔP – correction factor for the effective radiated power relative to the reference transmitter with EIRP=30 dBW, dB; PR – protection ratio, dB; ΔA – correction taking into account the spatial and polarization noise immunity of the receiving antenna (applies only to fixed reception), dB; OLC – combined location correction factor (used when protecting digital TV and radio broadcasting receivers), dB.

6. Repeating the actions of paragraph 5 for all sources of interference selected in paragraph 2 that are active or planned for use.

7. Calculation of the reference value of the used field strength (E_{fs}) at the j -th control point (6).

$$E_{fs} = 10 \lg \left(\sum_{n=1}^N 10 \frac{E_{fin}}{10} + 10 \frac{E_{min}}{10} \right), \quad (6)$$

where E_{fs} – reference value of the field strength used, dB($\mu\text{V/m}$), dB($\mu\text{V/m}$); E_{fin} – interfering field strength from the n -th service, dB($\mu\text{V/m}$); E_{min} – minimum used field strength of the protected electronic zone, dB($\mu\text{V/m}$); N – number of interference sources in the existing or planned network.

8. Checking the condition: $E_{us} \geq E_{fs}$.

If the condition is met, then a useful signal with a given quality is received at the control point, thereby forming a reference service area.

If the condition is not met, there is no reception of the useful signal, and reference service area is reduced.

9. The next control point is set within the service area of the existing or planned distribution network and steps 4-8 are carried out sequentially.

As a result, an array of control points is determined, located within the service area of the existing or planned for use service, corresponding to the boundaries of the reference service area.

10. Calculating results of the used field strength reference value at the control points of the reference service area are saved and are subsequently used when calculating EMC between existing and planned for use service and declared service.

Block diagram of the described algorithm for calculating the reference service area of the distribution network for television and radio broadcasting is shown in Figure 1.

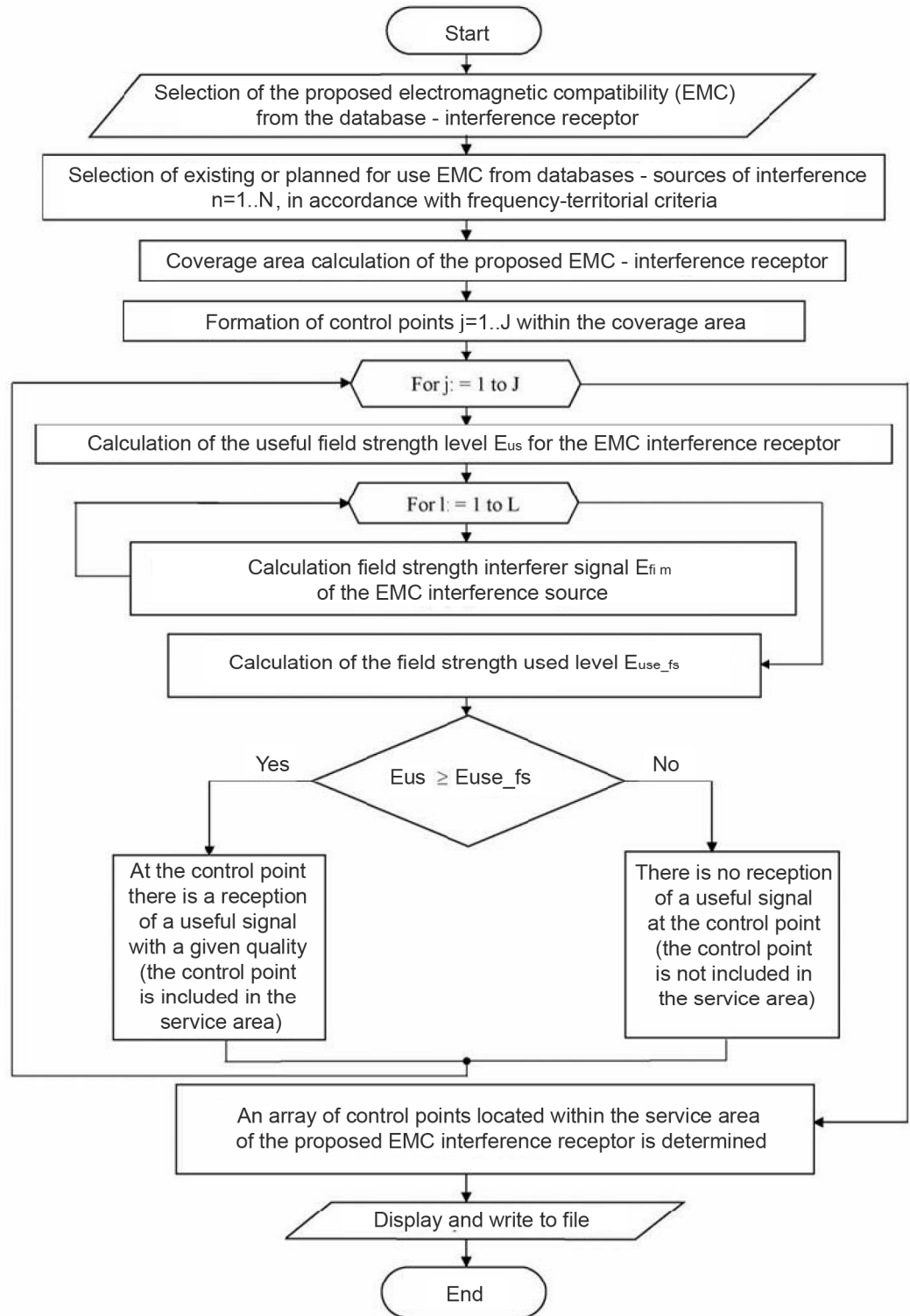


Fig. 1. Block diagram of the algorithm for calculating regional distribution network reference service area for television and radio broadcasting

3 Algorithm for calculating EMC between existing and planned for use service and declared service

The algorithm for calculating EMC between existing and planned for use service and declared service contains following stages:

1. Selecting the proposed service or a group of services forming SFN from the database and entering main initial data.
2. Formation of an array of existing or planned for use service interference receptors ($i=1\dots I$). Selection is carried out from the database using frequency-territorial criteria.
3. Formation of control points ($j=1\dots J$). Control points correspond to the places where radio distribution stations receive television and radio broadcasting and are located within the reference service area of the i -th operating or planned distribution zone and are determined in accordance with the algorithm for calculating the reference service area.
4. Calculation of the useful field strength at the j -th control point of the calculated reference service area of the i -th operating or planned for use service (1).
5. Calculation of the interfering field strength of the proposed service at the j -th control point of calculated reference service area of the i -th operating or planned service (3-5).
6. For the case of a group of claimed service forming an SFN, the value of the total interfering field from the specified service at the j -th control point is calculated (6).

$$E_{fi\ sum} = 10 \lg \left(\sum_{m=1}^M 10^{\frac{E_{fi\ m}}{10}} \right), \quad (6)$$

where $E_{fi\ sum}$ – the total strength of the interfering field from the services, forming SFN; $E_{fi\ m}$ is the strength of the interfering field from the m -th service included in the SFN; M is the number of services forming the SFN.

7. Determination of the reference value of the used field strength at the j -th control point in accordance with the algorithm for calculating the reference service area of the existing or planned distribution network.

8. Calculation of the reference field strength used at the j -th control point (7).

$$E_{use_fs} = 10 \lg \left(\sum_{i=1}^I 10^{\frac{E_{fi}}{10}} + 10^{\frac{E_{fs}}{10}} \right), \quad (7)$$

where E_{use_fs} – used field strength, dB(μ V/m); E_{fi} – interfering field strength from the i -th proposed service, dB(μ V/m); E_{fs} – reference value of the used field strength, dB(μ V/m); I – the number of declared services that form the SFN.

9. Calculation of the indicator “exceeding the used field strength” (8). Comparison with the permissible value of the indicator ΔE . The declared service (or a group of services that form the SFN) is compatible with the existing television and radio broadcasting network if the permissible value of the ΔE indicator is not exceeded at all control points on the border of the reference service areas of each protected service of the existing network.

$$\Delta E \geq E_{use_fs} - E_{fs}, \text{ dB}, \quad (8)$$

where ΔE – excess of the used field strength, dB; E_{use_fs} – used field strength at the reference point of the reference coverage area of the protected service of the existing network, taking into account the declared service, dB(μ V/m); E_{fs} – reference value of the field strength used, dB(μ V/m).

10. Checking the condition that the value of the used field strength does not exceed the value of the field strength of the useful station (9). The declared service (or a group of services forming the SFN) is compatible with the existing television and radio broadcasting network if this condition is met at all control points within the reference service areas of each protected service of the existing network.

If the EMC criteria are met (positive check of the conditions in paragraphs 9 and 10), the actions of paragraphs 4–10 are repeated at the next control point of the reference service area of the i -th operating or planned for use service.

$$E_{us} \geq E_{use_fs} \quad (9)$$

where E_{us} useful field strength for terrestrial television and radio broadcasting, dB(μ V/m); E_{use_fs} – used field strength at the reference point of the reference coverage area of the protected service of the existing network, taking into account the declared service, dB(μ V/m).

11. Repeat steps 3–10 for the remaining selected service – interference receptors.

12. The declared service (or a group of services forming the SFN) is compatible with the existing television and radio broadcasting network if the permissible value of the indicator ΔE is not exceeded at all control points on the border of the reference service areas, and the condition is met that the value of the used field strength does not exceed the value of the useful field strength stations at all control points within the reference service areas of each protected service of the existing network.

13. The calculation results are displayed on the screen and written to a special file.

If EMC conditions are not met, necessary measures are taken to limit the level of interference. Reducing the transmitter power, reducing the gain and introducing sectors in the antenna system, as well as changing the rating of the television or radio channel are considered as restrictive measures.

The block diagram of the described algorithm for calculating the EMC between the existing and planned for use service and the declared service is shown in Figure 2.

4 Algorithm for calculating service area of the proposed regional distribution network for television and radio broadcasting

The algorithm for calculating the service area of the proposed television and radio broadcasting distribution network contains the following steps:

1. Selecting the proposed service from the database and entering the main initial data.

2. Formation of an array of existing or planned for use service – sources of interference ($j=1\dots L$). The selection is carried out from the database using frequency-territorial criteria.

3. Formation of control points ($j=1\dots J$). The control points correspond to the places where radio electronic zones receive television and radio broadcasts and are located within the coverage area of the proposed radio electronic zone.

Calculations are carried out within the coverage area (ideal zone) of the proposed service, determined in accordance with the minimum used field strength of the service for television and radio broadcasting.

4. Calculation of the useful field strength (E_{us}) of the proposed service at the j -th control point (1).

5. Calculation of the interfering field strength (E_{fi}) from the l -th operating or planned for use service at the j -th control point (3-5).

6. Repeating the actions of p.5 for all sources of interference selected in p.2 that are active or planned for use.

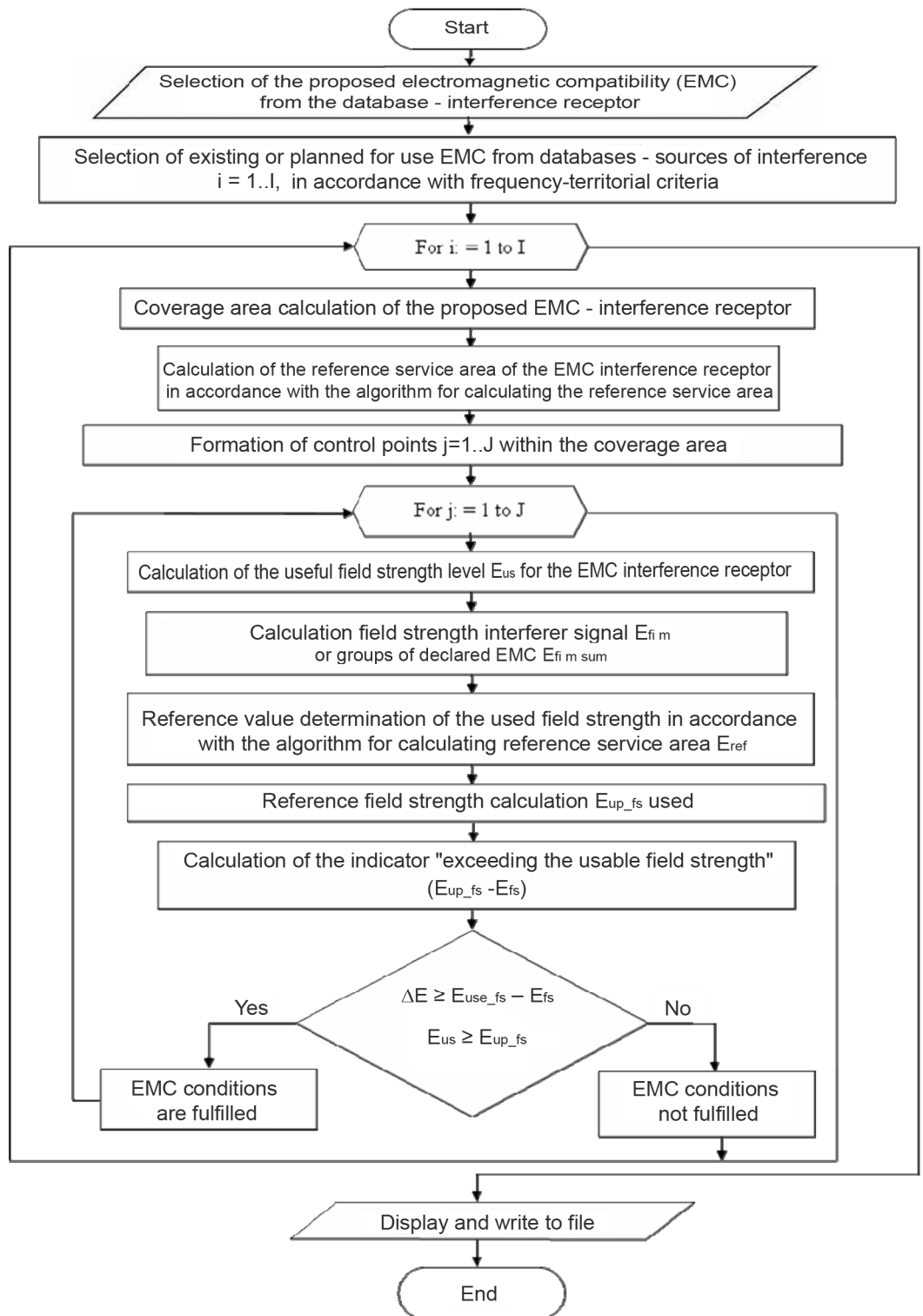


Fig. 2. Block diagram of the calculating EMC algorithm between existing and planned for use service and declared service

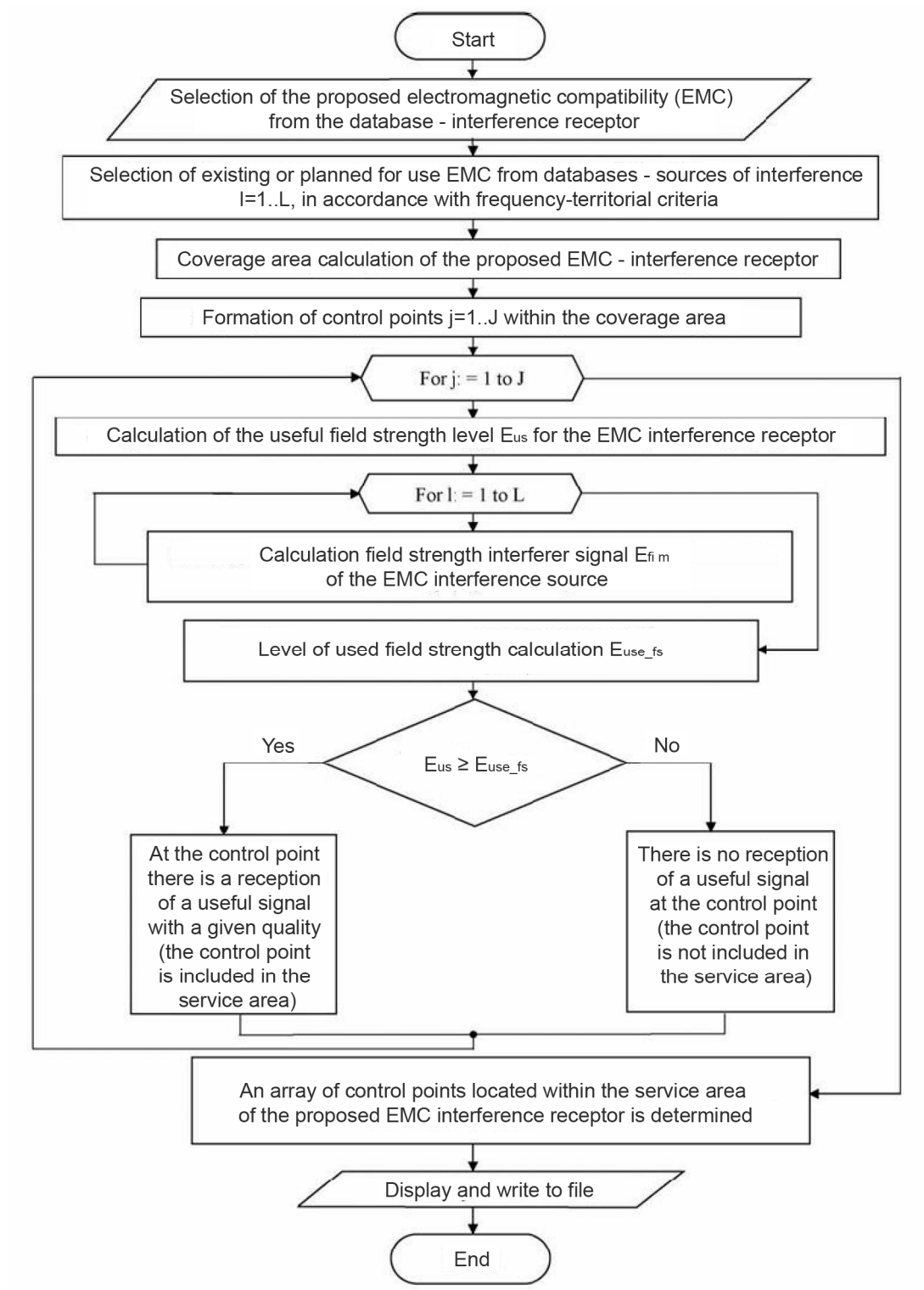


Fig. 3. Block diagram of the algorithm for calculating proposed service area

7. Calculation of the used field strength (E_{up}) at the j -th control point (10).

$$E_{up} = 10 \lg \left(\sum_{l=1}^L 10^{\frac{E_{fi}}{10}} + 10^{\frac{E_{min}}{10}} \right), \quad (10)$$

were E_{up} – used field strength for the declared service, dB(μ V/m); E_{fi} – interfering field strength from the l -th service, dB(μ V/m); E_{min} – minimum used field strength of the proposed service, dB(μ V/m); L – number of services (interference sources) in the existing or planned network.

8. Checking the condition: $E_{us} \geq E_{up}$.

If the condition is met, then at the control point the useful signal is received with a given quality, thereby forming a service area (area of reliable reception) of the proposed service.

If the condition is not met, there is no reception of the useful signal and the service area of the proposed service is reduced.

9. The next control point is set within the coverage area of the proposed service and steps 4-8 are carried out sequentially.

10. The calculation results are displayed on the screen and written to a special file, and the resulting service area is displayed on the screen.

For a group of declared service that form a SFN, the service area is determined sequentially for each services.

The block diagram of the described algorithm for calculating the service area of the proposed television and radio broadcasting distribution network is shown in Figure 3.

5 Conclusion

This article develop algorithms for calculating the reference service area of an existing or planned distribution network; to calculate EMC between existing and planned services and declared services; and to calculate the service area of the proposed television and radio broadcasting services. When protecting analogue and digital terrestrial television signals from simultaneous interference from several DAB+ blocks, it is advisable to carry out electromagnetic compatibility calculations and determine the conditions for using radio electronics separately for each DAB+ frequency block.

To determine the total interference impact from several DAB+ frequency blocks, the power addition method is used. A comparative analysis of the characteristics of digital radio broadcasting standards DAB and DAB+ (operating radio frequency bands, spectral masks, modulation methods, etc.) indicates their identity, with the exception of the applied audio signal coding method.

The procedures for processing the main digital streams, the structure of the transmission frame, the type of modulation, and the signal spectrum have not changed in the new version of the DAB+ digital broadcasting standard. Therefore, the values of the protective ratios considered as objects of influence from the DAB+ standard will also not change.

REFERENCES

- [1] The Chester 1997 Multilateral Coordination Agreement relating to Technical Criteria, Coordination Principles and Procedures for the introduction of Terrestrial Digital Video Broadcasting (DVB-T). Chester, 25 July 1997.
- [2] ETSI EN 302 755 V1.4.1 (2015-07) EUROPEAN STANDARD "Digital Video Broadcasting (DVB); Frame structure channel coding and modulation for a second generation digital terrestrial television broadcasting system (DVB-T2)".
- [3] Rep. ITU-R BT.2254-5 (11/2021) "Frequency and network planning aspects of DVB-T2", 2021.
- [4] Rec. ITU-R BT.1368-13 "Planning criteria, including protection ratios, for digital terrestrial television services in the VHF/UHF bands", 2017.
- [5] Rec. ITU-R BT.417-5 "Minimum field strengths for which protection may be sought in planning an analogue terrestrial television service", 2002.
- [6] Final Acts of the Regional Administrative Conference for the Planning of VHF Sound Broadcasting (Region 1 and Part of Region 3); Geneva 1984.
- [7] Rec. ITU-R BS.412-9 "Planning standards for terrestrial FM sound broadcasting at VHF", 1998.
- [8] Rec. ITU-R BS.704 "Characteristics of FM sound broadcasting reference receivers for planning purposes", 1990.
- [9] Rec. ITU-R BS.1114-12 "Systems for terrestrial digital sound broadcasting to vehicular, portable and fixed receivers in the frequency range 30-3 000 MHz", 2022.
- [10] Rec. ITU-R BS. BS.1660-9 "Technical basis for planning of terrestrial digital sound broadcasting in the VHF band", 2022.
- [11] Rep. ITU-R BS.2214-5 (10/2020) "Planning parameters for terrestrial digital sound broadcasting systems in VHF bands", 2020.
- [12] Final draft ETSI ES 201 980 V4.3.0 "Digital Radio Mondiale (DRM); System Specification", 2023.
- [13] F. Maier, A. Tissen and A. Waal, "Evaluation of the Channel Properties for a DRM+ System and Field Tests in the VHF-Band III (174-230 Mhz)," *2010 6th International Conference on Wireless and Mobile Communications*, Valencia, Spain, 2010, pp. 160-163, doi: 10.1109/ICWMC.2010.41.
- [14] F. Maier, A. Tissen and A. Waal, "Evaluations and measurements of a single frequency network with DRM+," *European Wireless 2012; 18th European Wireless Conference 2012*, Poznan, Poland, 2012, pp. 1-5.
- [15] Rec. ITU-R P.2001-5 "A general purpose wide-range terrestrial propagation model in the frequency range 30 MHz to 50 GHz", 2023.
- [16] K. Ulovec Analysis of Coexistence of DRM Plus and FM Broadcasting Systems. *Radioengineering*. Vol. 24, No. 4. December 2015. DOI: 10.13164/re.2015.1060.
- [17] A. V. Dolgopyatova and O. V. Varlamov, "Analysis of Long-Range VHF Radio Waves Propagation to Specify Protection Ratios Between Coexisting DRM+, RAVIS and IBOC Systems," *2021 Systems of Signal Synchronization, Generating and Processing in Telecommunications (SYNCHROINFO)*, 2021, pp. 1-4, doi: 10.1109/SYNCHROINFO51390.2021.9488392
- [18] Albrt Waal, "Coexistence of television broadcasting, fm broadcasting, digital broadcasting in DAB and DRM+ standards calculation methodology," *Synchroinfo Journal*, 2024, vol. 10, no. 1, pp. 18-23.

EFFICIENCY ANALYSIS OF SWITCHING CONVERTER-MODULATOR

Bayram Ibrahimov ¹, Oleg Varlamov ^{2,*}

¹ Azerbaijan Technical University, Baku, Azerbaijan;

bayram.ibrahimov@aztu.edu.az

<https://orcid.org/0000-0002-5364-1181>

² Institute of Radio and Information Systems (IRIS), Vienna, Austria;

ovarlamov@media-publisher.eu

<https://orcid.org/0000-0002-3996-9156>

* Correspondence: ovarlamov@media-publisher.eu

DOI: [10.36724/2664-066X-2024-10-2-12-20](https://doi.org/10.36724/2664-066X-2024-10-2-12-20)

ABSTRACT

Received: 10.03.2024

Accepted: 05.04.2024

Citation: Bayram Ibrahimov, Oleg Varlamov, "Efficiency analysis of switching converter-modulator," *Synchroinfo Journal* **2024**, vol. 10, no. 2, pp. 12-20

The article discusses methods of highly efficient linear RF power amplifier and transmitter design for future 5G/6G networks. Based on a consideration of various known methods for constructing high-efficiency power amplifiers, the prospects of developments using the envelope elimination and restoration (EER, or Kahn method) and envelope tracking (ET) method are substantiated. The prospects for implementing PWM switching converter-modulator for these methods are assessed. Based on the evaluation calculations performed, it is shown that this structure can potentially be used as an EEP/ET modulator for a number of 5G/6G applications and will have advantages over structures using class AB amplification.

Licensee IRIS, Vienna, Austria.

This article is an open access article distributed under the terms and conditions of the Creative Commons Attribution (CC BY) license (<https://creativecommons.org/licenses/by/4.0/>).



Copyright: © 2024 by the authors.

KEYWORDS: *Envelope elimination and restoration, Envelope tracking, High efficiency RF power amplifier, PWM Modulator.*

1 Introduction

Linear RF power amplifier (PA) and transmitter design is a large and extremely active research area for a wide range of applications in mobile and fixed radio technology, especially for future 5G/6G networks [1]. A number of linear transmitter techniques are available for commercial exploitation, with others at varying degrees of development [2, 3]. Therefore, it is possible to implement with current technology, many of degrees of freedom required in a flexible transmitter (for example, in terms of channel bandwidth, frequency coverage and required distortion performance). It is not possible yet to cover all of these requirements in a single, high-efficiency design.

The most popular techniques of PA's efficiency improvement are:

- Digital PA [4];
- Doherty system;
- Chireix – outphasing system [5];
- Polar modulation (Kahn – EER (envelope elimination and restoration) system) [6];
- Dynamic power supply voltage (envelope tracking – ET) [7-9];
- Dynamic current control (dynamic bias control);
- Hybrid methods [10-16].

Part 2 of this work describes the general characteristics of the methods presented above. It is shown that methods such as EER and ET with a switching mode PWM modulator can become most widespread for future applications. Part 3 provides a preliminary evaluation of the effectiveness of their use for the design of 5G/6G PA. Conclusions on the work are made in part 4.

2 Power Amplifier's Efficiency Improvement Methods

Digital PA consists of many elementary switching RF PAs that operate in classes D, E or F [4]. Its advantage (theoretically 100% DC to RF power conversion efficiency at all signal levels) can be realized in high power levels only (hundreds of W or kW approximately). Linearity of this technique decreases with back-off. A digital PA used in high power broadcast AM/DRM (Digital Radio Mondiale) transmitters with peak-to-average ratio of output power from 6 to 10 dB, and back-off below 6-9 dB.

Doherty system and Chireix – outphasing system (classical) offer improved average efficiency, but only over a limited range of back-off [19, 20] (Fig.1). These techniques were also common in high-power AM broadcast transmitters. They are being actively researched at present, but are not very suitable for wideband applications - both in terms of operating frequency and the width of modulating frequencies.

Chireix – outphasing system can used with Power Re-Use (recuperation) Technique (in microwave PAs) for improved efficiency at low output power levels (at 10 dB of back-off additionally) [21]. The lack of more widespread use can be attributed to its greater complexity and the need to employ different transmitter architecture. This technique can be analyzed in the future work.

The use of high-efficiency switching amplifiers again results in the potential of achieving 100% DC to RF power conversion efficiency and this is a major attraction of the technique. There are, however, a number of problems. First, the requirement for a cancellation process at the output of the transmitter results in stringent control requirements for the gain and phase matching of the two RF paths. This is one of the problems, which feedback mechanism employed in the CALLUM technique attempts to solve [22].

Secondly, the cancellation process itself, occurring as it does at the output of the amplifier, results in a potential loss of efficiency of up to 50%. This occurs if a hybrid power combiner is used in the summation process, as the cancelled power is then wasted in the 50 Ohm load connected to the difference port. The amount of power wasted will depend upon the modulation scheme in question, but this is still a significant problem with the technique.

Studying of the PAs with 80% efficiency shows that the resulting efficiency at the low power signal levels is similar to the same in class A. Let us have two channel amplifiers with the output power levels 0,25W (0,5W) and 80% efficiency for each of them. So, the power consumption will be 0,625W. Overall efficiency in this case will be 0,16% for 1mW output. The recuperation technique with 50% efficiency will increase the overall efficiency twice of previous example (0,32%).

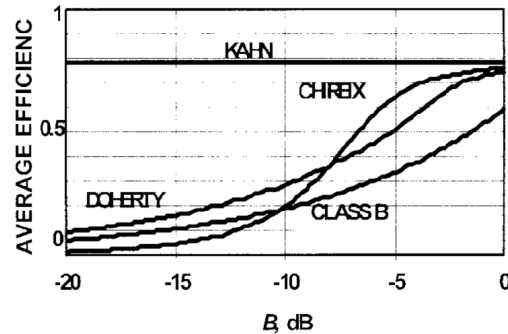


Fig. 1. Average efficiency of ideal PAs in back-off [23].

Kahn – EER system transmitter [6] operates with high efficiency over a wide dynamic range and, therefore, produces a high average efficiency for a wide range of signals and power back-off levels [23]. In either guise it has the potential, theoretically at least, to achieve 100% DC to RF power conversion efficiency at all envelope levels of the modulation signal.

The potential for high levels of efficiency stems from the fact that the RF power amplifier is freed from the requirement to amplify envelope varying signals and thus can be implemented by one of the switching RF power amplifier classes (e.g. class-D, E or F). Similarly the 'audio frequencies' (AF) envelope amplifier, which is effectively supplying the 'DC' power to the RF amplifier (and thereby applying high-level amplitude modulation), can be implemented by a switching audio amplifier technique (e.g. pulse-width modulation (PWM), class-S). As both of these types of amplifier are theoretically 100% efficient, and as there are (ideally) no other loss mechanisms (e.g. couplers or delay-lines) in the high-power RF path, the overall amplifier could be 100% efficient. Clearly a practical realisation will fall short of this goal, but a 20% implementation margin (in efficiency terms) would still result in an 80% efficient linear amplifier – a highly-desirable result.

Practical EER transmitters have been built for a number of applications, however there are a lot of practical problems which limit, in particular, the linearity available from the system. The use of high-level modulation of the power supply is not a particularly linear method of modulating an RF carrier, especially at low envelope levels (and power back-off), where the RF power transistor will cut-off introducing significant distortion. Furthermore, the switching frequency of the AF PWM amplifier must be at least 5...10 times exceeding of the RF signal bandwidth. With 5 MHz signal bandwidth the switching frequency of AF amplifier must be greater than 50 MHz. This is the very difficult task to solve it with high efficiency.

However, this technique has got a high potential for 5G/6G systems and will be studied in the future. Estimation of an opportunity of realization switching DC-DC converter on high frequencies will present at ch. 3.

Dynamic power supply voltage (envelope tracking) system has theoretical efficiency less than the EER systems but provides a good linearity at all power levels because of RF PA capability to operate in AB class. In this case, an AF amplifier is less difficult to realize than EER because its amplitude variation is smaller. There are still problems with signal filtering due to the harmonics of the AF amplifier. An example of efficiency improvement for this technique is presented in Figure 2 [24].

It can be proposed slow supply voltage control in tie with output power level. This approach results in efficiency decreasing (it still higher than the same in A or AB classes) but also gives significant simplification of an AF amplifier design, what can be explained by fact that bandwidth of amplifier will be defined by the rate of output power switching.

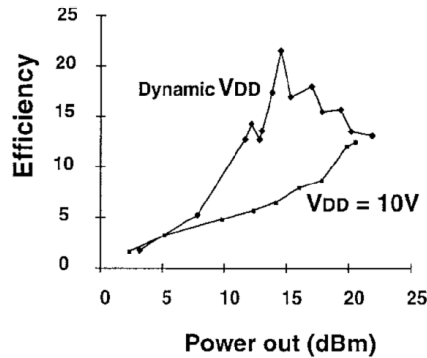


Fig. 2. Measured efficiency versus output power for dynamic supply amplifier and for a comparable amplifier with fixed VDD [24].

Dynamic current control (dynamic bias control)

This method has the lowest efficiency of previous studying, but is ease of design. Low power of controlling signals gives possibility to realize this structure in a single PA IC. The simplest application of this method is the bias current switching at low power operations (low power mode). This application has been realized in some of the modern PA ICs. This resulted in efficiency increasing of about 7% at $P_{out} = 16\text{dBm}$.

3 Estimation of an opportunity of realization switching DC-DC converter on high frequencies

Switching regulators and modulators based on Pulse Width Modulation (PWM) find wide application in engineering of the communications due to their high efficiency. Clock frequencies of produced and developed similar devices usually do not exceed 0.4 ... 3.0 MHz. At such low clock frequencies the output filter should have big inductances (about few μH) and capacitors (about few μF) with large PCB area.

There are known switching DC-DC converters without use inductance based on overcharge of capacitors (charge pump). However similar devices have high output impedance and consequently work with small output current.

In the present section it will be carried out the theoretical researches of influence of the basic parameters of MOS transistors and clock frequency on PWM modulator efficiency.

Statement of a task.

The analysis will be made using the block diagram shown on a Figure 3, which represents the synchronous converter on complementary MOS transistors. The basic losses in such structure are commutative (switching) loss P_{com} on overcharge of transistor capacities and loss in resistors R_{on} of open transistors.

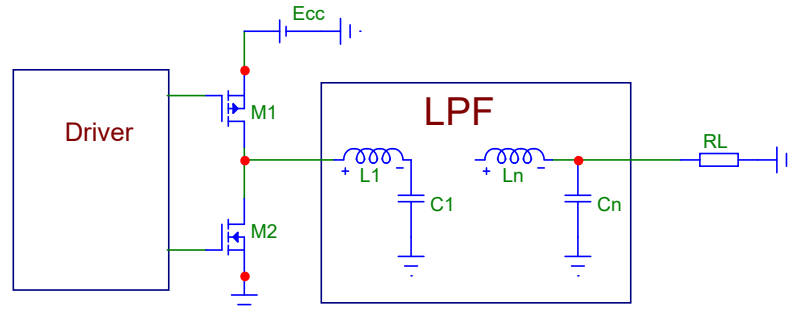


Fig. 3. DC-DC with PWM

Commutative loss of two transistors M1 and M2 at a rectangular drive voltage swing from 0 to E_{cc} on each gate and drain of transistors is defined by his total capacity (input and output), clock frequency F_0 and input voltage E_{cc} :

$$P_{comm} = F_0 * C * E_{cc}^2.$$

Losses on resistors of open transistors R_{on} , in the assumption, that they are equal, are defined by the following expression:

$$P_R = I_L^2 * R_{on} = P_{out} * (R_L + R_{on} / R_L), \text{ where:}$$

I_L - constant current in load R_L ;

$$P_{out} = U_L^2 * R_L \text{ - output power of DC current in load } R_L.$$

The maximum available efficiency of the output stage is defined by the ratio of output P_{out} and consumed P_0 powers:

$$\eta = P_{out} / P_0 = P_{out} / (P_{out} + P_{com} + P_R).$$

The simulation results of DC efficiency vs P_{out} are given on the diagrams of a Figures 4-7. On Figures 5-7 total capacity $C=900$ pF corresponds to power MOS transistors (similar to IRFZ24N, IRF9Z24N with $C=900$ pF; $R_{on}=0.1$ Ohm), and total capacity $C=200$ pF corresponds new technologies with $C=200$ pF; $R_{on}=0.1$ Ohm.

Similar dependences of efficiency for linear regulator of a compensation type (Lin DC-DC), calculated based on following expression:

$$\eta_{LIN} = P_{out} / P_0 = \sqrt{(P_{out} * R_L)} / E_{CC}.$$

In both cases the maximal DC output voltage on load R_L is defined by:

$$U_{L_{max}} = E_{CC} * (R_L + R_{on} / R_L).$$

It is important to note, that except for the losses, considered above of lowering efficiency, there are also others losses with which it is possible to struggle technological and circuit technique methods.

One of such reason is through current proceeding through transistors, if his both are open or in active mode. For prevention of this effect it is necessary to design the driver so that between unlocking pulses on gates of MOS transistors there was a small time interval.

The second reason of additional losses is the internal resistance (R_G) in a gate circuit of the MOS transistors, which together with input capacity C_{GS} forms integrating RC circuit. This circuit increases times of front and recession of pulses drain current, during which the transistors work in active mode, that also results in efficiency decrease. According to said above special attention by transistors selection should be paid to low value of R_G .

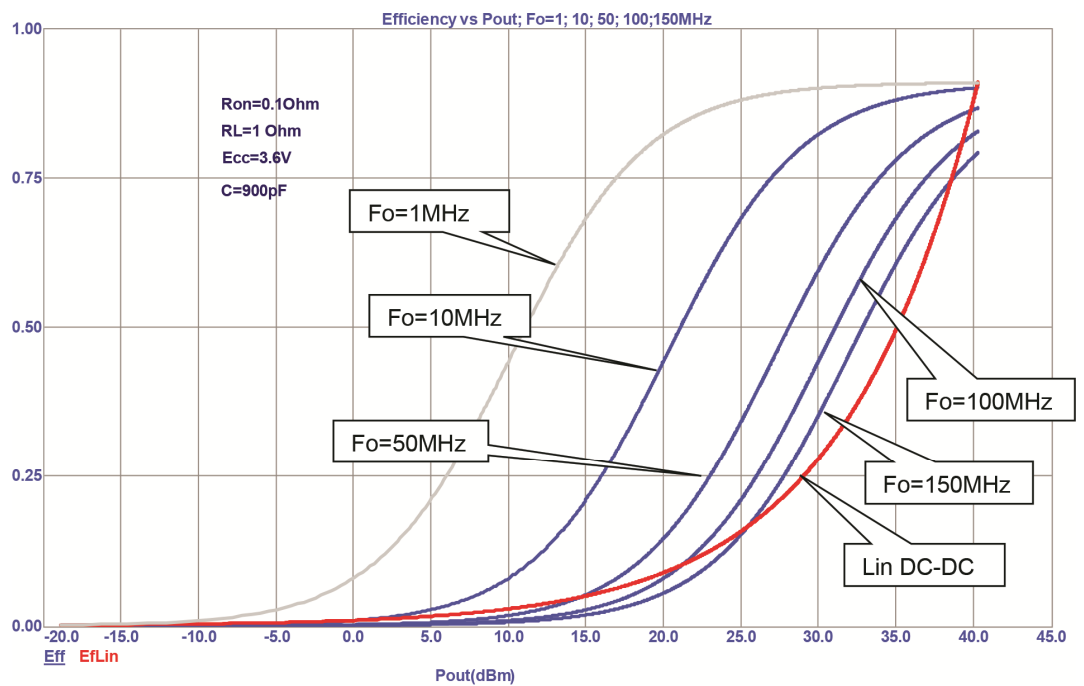


Fig. 4. Dependence of efficiency linear (red line) and PWM modulator (blue lines) vs output DC power (dBm) at various PWM clock frequencies: $F_o=1$; 10; 50; 100; 150 MHz. (Power MOS transistors similar to IRFZ24N, IRF9Z24N with $C=900\text{ pF}$; $R_{on}=0.1\text{ Ohm}$) and $R_L=1\text{ Ohm}$; $E_{cc}=3.6\text{ V}$.

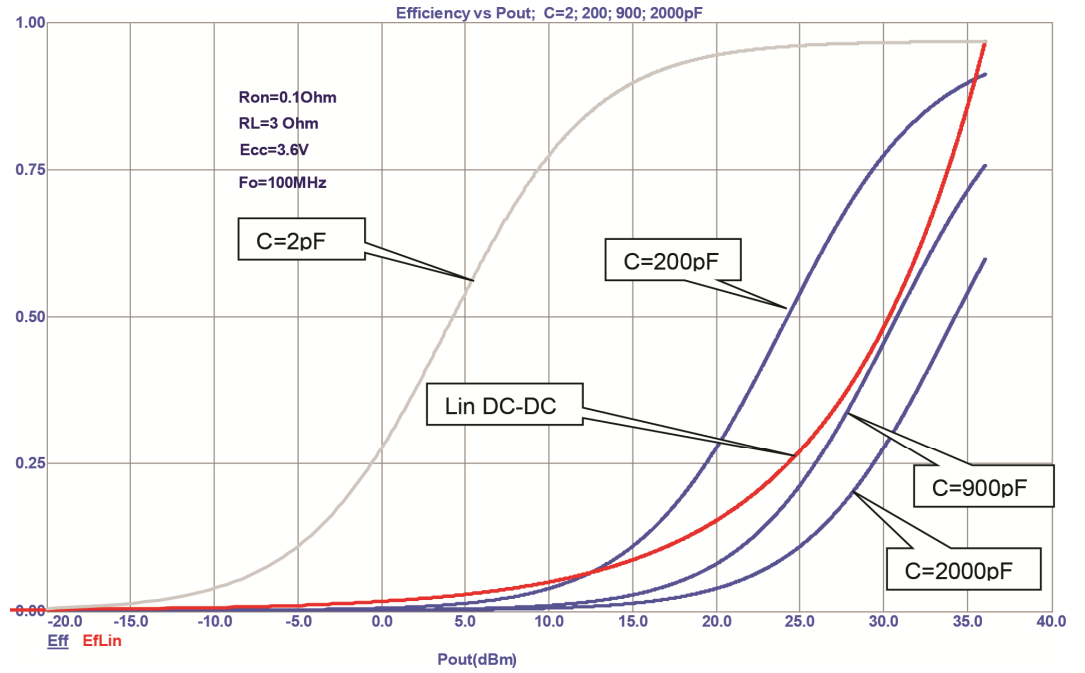


Fig. 5. Dependence of efficiency linear (red line) and PWM modulator (blue lines) vs output DC power (dBm) at various capacities of PWM transistors: C=2; 200; 900; 2000; pF. $F_o=100$ MHz; $R_{on}=0.1$ Ohm; $R_L=3$ Ohm; $E_{cc}=3.6$ V.

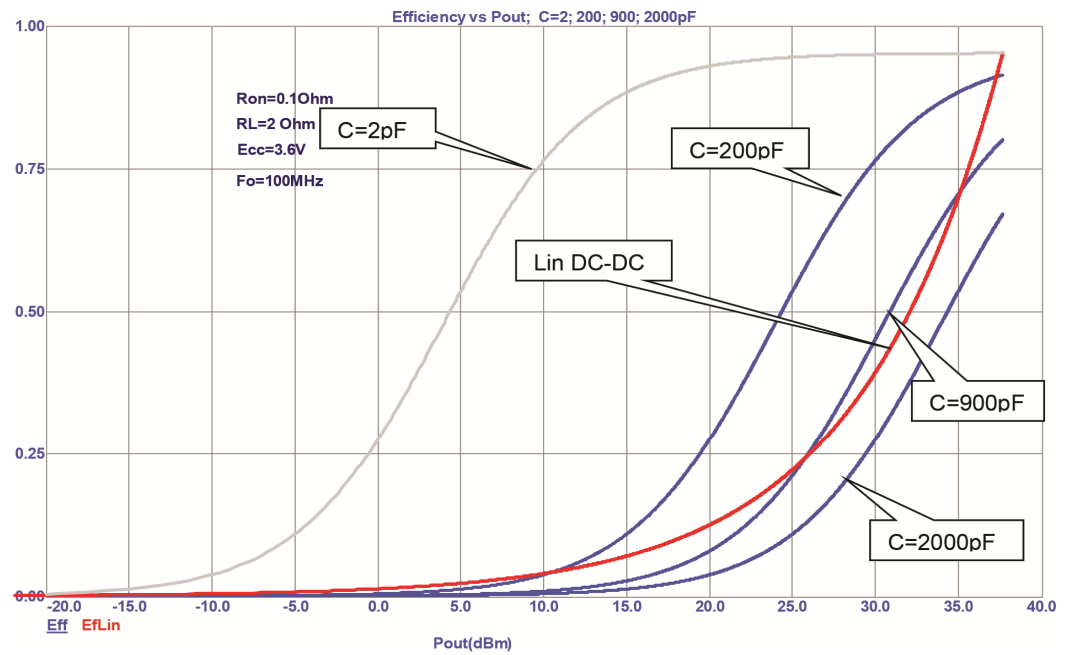


Fig. 6. Dependence of efficiency linear (red line) and PWM modulator (blue lines) vs output DC power (dBm) at various capacities of PWM transistors: C=2; 200; 900; 2000; pF. $F_o=100$ MHz; $R_{on}=0.1$ Ohm; $R_L=2$ Ohm; $E_{cc}=3.6$ V.

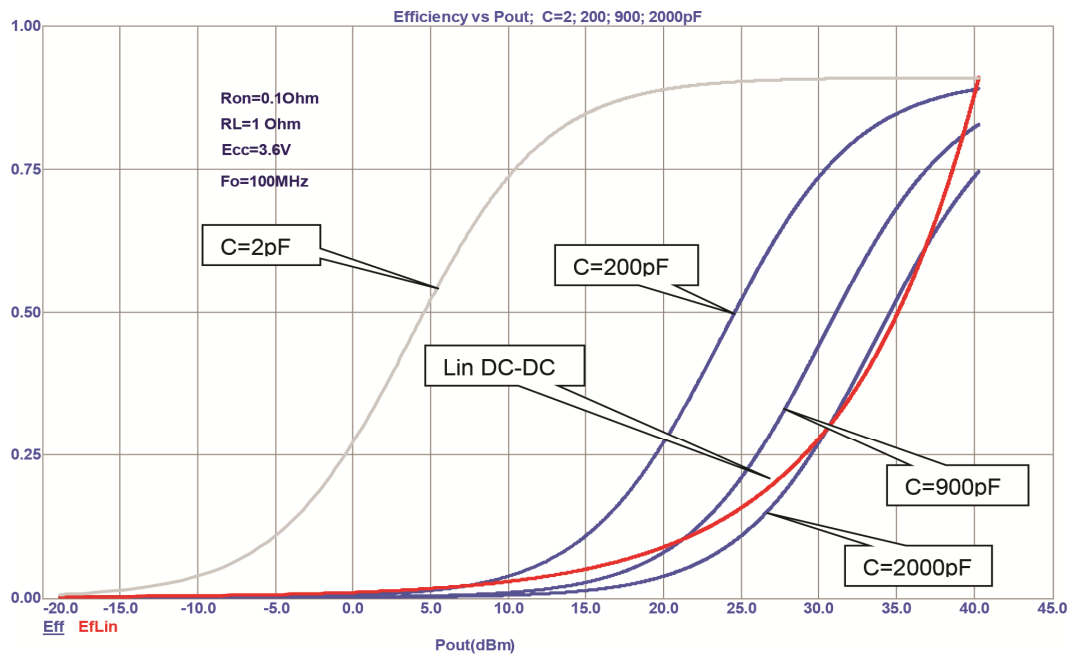


Fig. 7. Dependence of efficiency linear (red line) and PWM modulator (blue lines) vs output DC power (dBm) at various capacities of PWM transistors: C=2; 200; 900; 2000; pF. $F_o=100\text{ MHz}$; $R_{on}=0.1\text{ Ohm}$; $R_L=1\text{ Ohm}$; $E_{cc}=3.6\text{ V}$.

From the results given above follows, that the basic reason of efficiency decrease in PWM modulator on high clock frequencies are the capacities of transistors.

However with total capacity of transistors pair $C = 200\text{ pF}$ the limiting efficiency of the PWM modulator on frequencies $F_o \approx 100\text{ MHz}$ are higher than at the linear modulator at output power range from $\approx 10\text{ mW}$ to $5 \dots 10\text{ W}$ with load from 1 to 3 Ohm .

This structure can potentially be used as an EEP/ET modulator for a number of 5G/6G applications.

4 Conclusion

- Methods for improving the energy efficiency of 5G/6G PA are considered.
- An assessment of the feasibility of implementing a DC-DC switching converter at high frequencies has been developed. This structure can potentially be used as an EEP/ET modulator for a number of 5G/6G applications.

REFERENCES

- [1] A. Pastukh, V. Tikhvinskiy, S. Dymkova, and O. Varlamov, "Challenges of Using the L-Band and S-Band for Direct-to-Cellular Satellite 5G-6G NTN Systems," *Technologies*, vol. 11, no. 4, p. 110, Aug. 2023, doi: 10.3390/technologies11040110.
- [2] R. Caverly, F. Raab, J. Staudinger, "High-Efficiency Power Amplifiers," *IEEE Microw. Mag.* 2012, 13, pp. 22-32. doi: 10.1109/MMM.2012.2216716.
- [3] A. Grebennikov, M.J. Franco, "Switchmode RF and Microwave Power Amplifiers," Academic Press: London, UK, 2021.
- [4] O.V. Varlamov, I.A. Goncharov and V.G. Lavrushenkov, "High-power HF digital-analog converter for SSB signal power amplifiers," *Telecommunications and Radio Engineering*, vol. 44, no. 8, pp. 49, 1989.
- [5] H. Chireix, "High power outphasing modulation," *Proc. IRE*, 1935, 23, pp. 1370-1392. doi: 10.1109/JRPROC.1935.227299.
- [6] L. Kahn, "Single-sideband transmission by envelope elimination and restoration," *Proc. IRE*, 1952, no. 40, pp. 803-806. doi: 10.1109/JRPROC.1952.273844.
- [7] P. Asbeck, Z. Popovic, "ET comes of age: Envelope tracking for higher-efficiency power amplifiers," *IEEE Microw. Mag.* 2016, no. 17, pp. 16-25. doi: 10.1109/MMM.2015.2505699.

-
- [8] G.P. Gibiino, J. Couvidat, G. Avolio, D. Schreurs, A. Santarelli, "Supply-terminal 40 MHz BW characterization of impedance-like nonlinear functions for envelope tracking PAs," *Proceedings of the ARFTG Microwave Measurement Conference*, San Francisco, CA, USA, 27 May 2016; pp. 1-4.
- [9] P. Chen, A. Alt, J. Moreno Rubio, S. Alsahali, J. Lees, R. Quaglia, M. Casbon, P.J. Tasker, "Optimizing Linearity of Envelope Tracking Power Amplifier Using Baseband Linearization Approach," *Proceedings of the 2020 International Workshop on Integrated Nonlinear Microwave and Millimetre-Wave Circuits (INMMiC)*, Cardiff, UK, 16-17 July 2020.
- [10] O.V. Varlamov, D.C. Nguyen and S.E. Grychkin, "Simultaneous Application of Several Synthetic Methods for High Efficiency Radiofrequency Amplification," *2021 Systems of Signals Generating and Processing in the Field of on Board Communications*, 2021, pp. 1-5, doi: 10.1109/IEEECONF51389.2021.9416126.
- [11] Y.-T. Hsu, Z.-Y. Lin, J.-J. Lee, K.-H. Chen, "An envelope tracking supply modulator utilizing a GAN-based integrated four-phase switching converter and average power tracking-based switch sizing with 85.7% efficiency for 5G NR power amplifier," *IEEE J. Solid-State Circuits* 2021, no. 56, pp. 3167–3176. doi: 10.1109/JSSC.2021.3079403.
- [12] O.V. Varlamov, "Multiphase PWM characteristics in the EER transmitter envelope path," *2021 International Conference on Engineering Management of Communication and Technology (EMCTECH)*, 2021, pp. 1-5, doi: 10.1109/EMCTECH53459.2021.9619166.
- [13] D. Kim, J.-S. Bang, J. Baek, S. Park, Y.-H. Jung, J. Han, I.-H. Kim, S.-Y. Jung, T. Nomiya, J.-S. Paek, et al., "33.9 a hybrid switching supply modulator achieving 130 MHz envelope-tracking bandwidth and 10 W output power for 2G/3G/LTE/NR RF Power Amplifiers," *Proceedings of the 2021 IEEE International Solid-State Circuits Conference (ISSCC)*, San Francisco, CA, USA, 13–22 February 2021.
- [14] J.-S. Bang, D. Kim, J. Lee, S. Jung, Y. Choo, S. Park, Y.-H. Jung, J.-Y. Ko, T. Norniyama, J. Baek, et al., "2-TX digital envelope-tracking supply modulator achieving 200 MHz channel bandwidth and 93.6% efficiency for 2G/3G/LTE/NR RF Power Amplifiers," *Proceedings of the 2022 IEEE International Solid-State Circuits Conference (ISSCC)*, San Francisco, CA, USA, 20-24 February 2022.
- [15] T. Cappello, T.W. Barton, C. Florian, M. Litchfield, Z. Popovic, "Multilevel Supply-Modulated Chireix Outphasing With Continuous Input Modulation," *IEEE Trans. Microw. Theory Tech.* 2017, no. 65, pp. 5231-5243. doi: 10.1109/TMTT.2017.2756038.
- [16] C.-H. Kuo, J.-T. Yeh, J.-H. Chen, Y.-J.E. Chen, "A Dual-Phase Center-Aligned 7-Bit Digital Pulsewidth Modulator for Polar Transmitters," *IEEE Trans. Microw. Theory Tech.* 2022, no. 70, pp. 5205-5212. doi: 10.1109/TMTT.2022.3205586.
- [17] O. Varlamov, D.C. Nguyen, and A. Grebennikov, "Broadband and Efficient Envelope Amplifier for Envelope Elimination and Restoration/Envelope Tracking Higher-Efficiency Power Amplifiers," *Sensors*, vol. 22, no. 23, p. 9173, Nov. 2022, doi: 10.3390/s22239173.
- [18] S.E. Grychkin, A.M. Zakharov and O.V. Varlamov, "Calculation and Simulation of GaN FET Modulator for Envelope Elimination and Restoration Power Amplifier," *2023 Systems of Signal Synchronization, Generating and Processing in Telecommunications (SYNCHROINFO)*, Pskov, Russian Federation, 2023, pp. 1-7, doi: 10.1109/SYNCHROINFO57872.2023.10178469.
- [19] F.H. Raab, "Efficiency of Doherty RF Power-Amplifier Systems," *IEEE Transactions on Broadcasting*, vol. BC-33, no. 3, pp. 77-83, Sept. 1987, doi: 10.1109/TBC.1987.266625.
- [20] F. Raab, "Efficiency of Outphasing RF Power-Amplifier Systems," *IEEE Transactions on Communications*, vol. 33, no. 10, pp. 1094-1099, October 1985, doi: 10.1109/TCOM.1985.1096219.
- [21] R. Langridge, T. Thornton, P.M. Asbeck and L.E. Larson, "A power re-use technique for improved efficiency of outphasing microwave power amplifiers," *IEEE Transactions on Microwave Theory and Techniques*, vol. 47, no. 8, pp. 1467-1470, Aug. 1999, doi: 10.1109/22.780396.
- [22] D.J. Jennings and J.P. McGeehan, "A high-efficiency RF transmitter using VCOderived synthesis: CALLUM," *IEEE Transactions on Microwave Theory and Techniques*, vol. 47, pp. 715-721, June 1999.
- [23] F.H. Raab, B.E. Sigmon, R.G. Myers and R.M. Jackson, "L-band transmitter using Kahn EER technique," *IEEE Transactions on Microwave Theory and Techniques*, vol. 46, no. 12, pp. 2220-2225, Dec. 1998, doi: 10.1109/22.739200.
- [24] G. Hanington, Pin-Fan Chen, P.M. Asbeck and L.E. Larson, "High-efficiency power amplifier using dynamic power-supply voltage for CDMA applications," *IEEE Transactions on Microwave Theory and Techniques*, vol. 47, no. 8, pp. 1471-1476, Aug. 1999, doi: 10.1109/22.780397.

INFORMATION MODEL OF VEHICLE TELEMATICS DATA CLUSTER COLLECTION USING UAV

Mamedov Shamsi Elshan ogly¹, Rahimov Elshan Rasif ogly²,

¹ National Aerospace Agency, Baku, Azerbaijan;

² Baku Higher Oil School, Baku, Azerbaijan

ABSTRACT

Telematics is a set of basic systems that provide services in accordance with user needs. Telematics systems can be classified according to the areas of tasks performed: monitoring the condition of the road, managing the flow of traffic, providing information services to road users, etc. Telematics also allows you to monitor the condition of vehicles or their cargo using remote monitoring methods and technologies. The use of telematic systems and technologies allows for real-time management of transport systems. The article is devoted to the development of an information model for collecting motor transport telematics data using unmanned aerial vehicles. A model of the V2R network type is considered in which one car in the cluster is defined as a central node that receives telematic information from other cars in the cluster and then transmits the collected information to the base station. It is proposed to replace the central vehicle with a specialized UAV that collects telematic information from all vehicles in the cluster and transmits the collected information to the base station. A formula has been obtained to calculate the maximum amount of information that can be collected and transmitted to the base station.

DOI: [10.36724/2664-066X-2024-10-2-21-27](https://doi.org/10.36724/2664-066X-2024-10-2-21-27)

Received: 20.03.2024

Accepted: 15.04.2024

Citation: Mamedov Shamsi Elshan ogly, Rahimov Elshan Rasif ogly, "Information model of vehicle telematics data cluster collection using UAV," *Synchroinfo Journal* 2024, vol. 10, no. 2, pp. 21-27

Licensee IRIS, Vienna, Austria.

This article is an open access article distributed under the terms and conditions of the Creative Commons Attribution (CC BY) license (<https://creativecommons.org/licenses/by/4.0/>).



Copyright: © 2024 by the authors.

KEYWORDS: *telematics, cluster, UAV, drones, optimization, information collection, base station.*

1 Introduction

As noted in [1], telematics is an ever-increasing element of complex integrated systems for performing certain transport tasks. Telematics is a set of basic systems that provide services in accordance with user needs. According to [2], telematics systems can be classified according to the areas of tasks performed, such as monitoring the condition of the road, managing the flow of traffic, providing information services to road users, etc. Telematics also allows you to monitor the condition of vehicles or their cargo using remote monitoring methods and technologies. According to [3], the use of telematic systems and technologies makes it possible to manage transport systems in real time.

As noted in [4], to achieve safety and productivity (performance), intelligent transportation systems are being developed, based on telematics and vehicle systems. To transmit data in telematics systems, wireless communications and network technologies such as IEEE 802.11 (WiFi), IEEE 802.16 (WiMAX), etc. are used. In intelligent transport systems, communications such as “vehicle-to-road” (V2R), and vehicle-to-vehicle (V2V). V2R communications include vehicle nodes and road base stations. This communication model can use WiFi, WiMAX and DSRC technologies. In particular, using DSRC technology (short range communication technology), each vehicle is equipped with an on-board unit (OBUS), which can receive or transmit information to road base stations [5]. It is possible that some OBUS create a group where all the information from nearby vehicles is first transmitted to one selected vehicle, which then sends all the collected information to the base station. The model of such cluster data transmission is shown in the diagram shown in Figure 1.

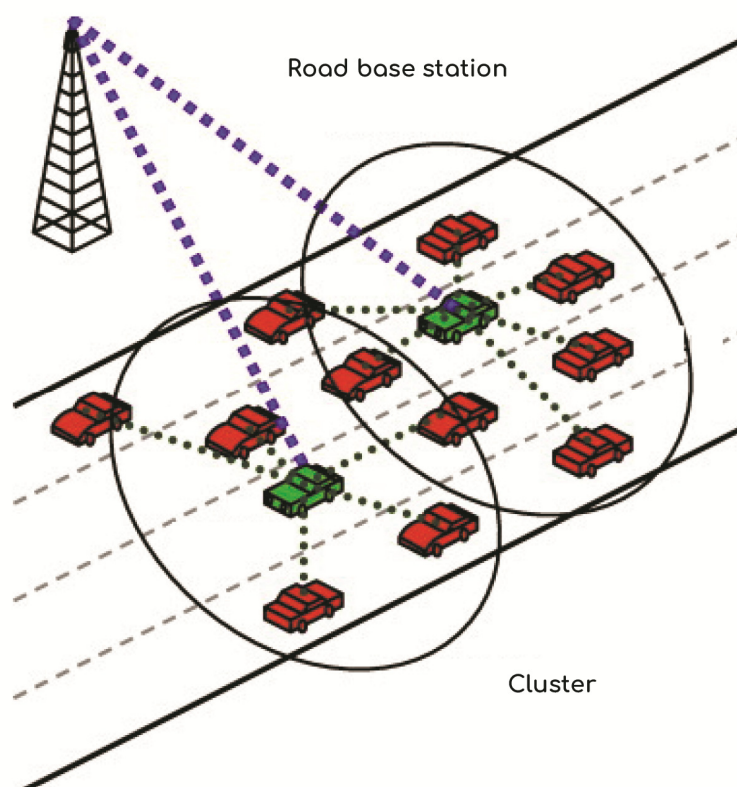


Fig. 1. Model of data transmission cluster organization in V2R networks

At the same time, it seems to us that using any car as a receiving unit for an entire cluster of cars is an impractical solution, because Some cluster of cars, passing near the next base station, must contain sufficiently reliable receiving and transmitting equipment. Moreover, due to the random nature of the occurrence of such clusters, almost all cars must carry such equipment, because any cluster element can be in the position of the central element of the cluster. To eliminate such inconveniences and excesses, a scheme can be proposed. Where the role of the central element of a certain cluster is performed by an unmanned aerial cluster data collection is shown in Figure 2 [6]. At the same time, as noted in [7, 8], UAVs can also be used as base stations.

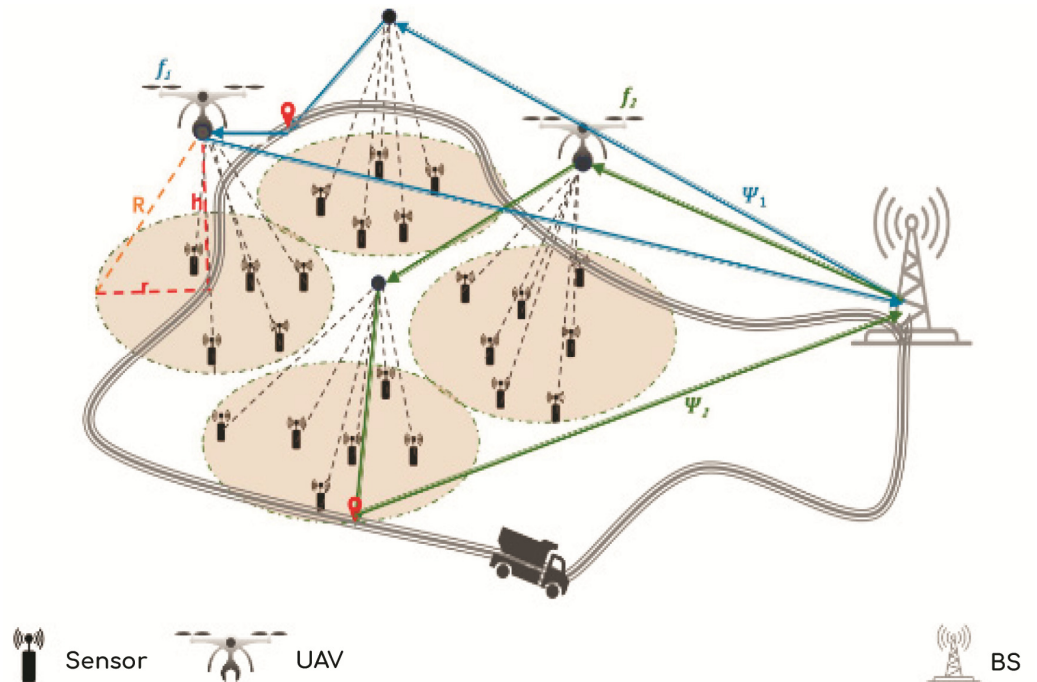


Fig. 2. Scheme of using UAVs to collect information from individual elements of a certain cluster [6]

It should be noted that in [6] it was analyzed in detail from the perspective of calculating energy consumption.

2 Materials and methods

Let's consider a two-stage data transmission model of the above-mentioned telematics system for transmitting and collecting data using UAVs as the central elements of clusters within which a wireless network is organized. A schematic representation of the bottom stage of a two-stage telematics network is shown in Figure 3.

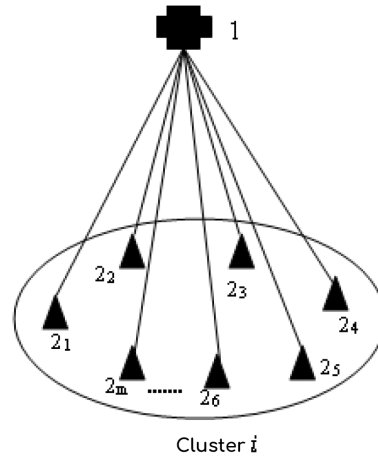


Fig. 3. Scheme of the lower stage of cluster data collection in a two-stage telematics system. The numbers indicate: 1 – UAV; $2_i; i = \overline{1, n}$ – transmitting nodes of cluster cars

The limit analysis and assessment of information flows in this scheme will be carried out on the basis of the classical Shannon formula and variational optimization methods. We define the amount of information transmitted from the i -th car to the j -th UAV as

$$M_{i,j} = N_{i,j} \cdot \log_2 \frac{I_0}{\sigma_j} \quad (1)$$

where $N_{i,j}$ – number of pulses whose amplitude can have one of I_0/σ_j number of positions, where I_0 – the maximum possible signal amplitude; σ_j – UAV receiver noise.

If we take into account that all the cars on the road dynamically form a certain cluster, then in order to obtain reliable spatio-temporal information it is necessary to maintain simultaneous parallel communication with all cars. In this case, if we take into account that the number of pulses in the information message from a specific car to the UAV depends on the controlled parameters of the car, then we can assume that the total noise during data transmission of the i -th car will depend on $N_{i,j}$. Consequently, formula (1) takes the form

$$M_{i,j} = N_{i,j} \cdot \log_2 \frac{I_0}{\sigma_j(N_{i,j})} \quad (2)$$

Further, if we assume that in each randomly selected cluster j the set of cars is such that their indicators $N_{i,j}$ form an ordered set N_j , where

$$N_j = \{N_{1,j}; N_{2,j}; N_{3,j}; \dots; N_{m,j}\} \quad (3)$$

in which $N_{i,j} = N_{i-1,j} + N_j$; $i = \overline{1, m}$; $N_{0,j} = 0$.

Therefore, we define the amount of information transmitted from one j -th cluster to the j -th UAV as

$$M_j = \sum_{i=1}^m N_{i,j} \cdot \log_2 \frac{I_0}{\sigma_j(N_{i,j})} \quad (4)$$

At the same time, it can be required that the total noise when connecting all cars does not exceed the value of C_1 . Therefore, we have

$$\sum_{i=1}^m \sigma_j(N_{i,j}) dN_{i,j} = C; \quad C = const \quad (5)$$

As a first approximation, we write discrete models (4) and (5) in continuous form. We rewrite model (4) as

$$M_{jm} = \int_0^{N_{jmax}} N_j \cdot \log_2 \frac{I_0}{\sigma_j(N_{i,j})} dN_j \quad (6)$$

Let us represent model (5) in continuous form as

$$\int_0^{N_{jmax}} \sigma(N_j) dN_j = C \quad (7)$$

Based on models (6) and (7), we create a variational optimization problem whose objective functional F_1 has the form

$$F_1 = \int_0^{N_{jmax}} N_j \cdot \log_2 \frac{I_0}{\sigma_j(N_{i,j})} dN_j + \lambda \left[\int_0^{N_{jmax}} \sigma(N_j) dN_j - C \right] \quad (8)$$

where λ – Lagrange multiplier.

According to [9], the solution to problem (8) must satisfy the condition

$$\frac{d \left\{ N_j \cdot \log_2 \frac{I_0}{\sigma_j(N_{i,j})} + \lambda(N_j) \right\}}{d\sigma(N_j)} = 0 \quad (9)$$

From condition (9) we obtain

$$\frac{N_j}{C_1} \cdot \frac{1}{\sigma_j(N_j)} + \lambda = 0 \quad (10)$$

where C_1 – constant for converting binary logarithm to natural logarithm.

From (10) we obtain

$$\sigma_j(N_j) = -\frac{N_j}{\lambda C_1} \quad (11)$$

Taking into account (7) and (11) we find

$$-\int_0^{N_{jmax}} \frac{N_j}{\lambda C_1} dN_j = C \quad (12)$$

From expression (12) we have

$$\lambda = -\frac{N_{j\max}^2}{2CC_1} \quad (13)$$

Inserting (13) into (11) we get

$$\sigma_j(N_j) = \frac{2CN_j}{N_{j\max}^2} \quad (14)$$

When solving (14), the functional $F1$ reaches a maximum, since the derivative (10) with respect to $\sigma_j(N_j)$ turns out to be a negative value.

Taking into account (6) and (14), it can calculate the maximum value M_{jm} , i.e.

$$M_{jm,\max} = \int_0^{N_{j\max}} N_j \cdot \log_2 \frac{I_0 N_{j\max}^2}{2CN_j} dN_j = \frac{N_{j\max}^2}{2} \log \frac{I_0 N_{j\max}^2}{2C} + \int_0^{N_{j\max}} N_j \cdot \log_2 \frac{1}{N_j} dN_j \quad (15)$$

Having designated

$$\int_0^{N_{j\max}} N_j \cdot \log_2 \frac{1}{N_j} dN_j = C_2$$

Let's write

$$M_{jm,\max} = \left[\log \frac{I_0 N_{j\max}^2}{2C} \right] \frac{N_{j\max}^2}{2} + C_2 \quad (16)$$

Thus, the maximum amount of information coming from one cluster to the input of the base station can be estimated using formula (16).

3 Discussion

A cluster model for collecting telematic information transmitted to a base station is analyzed. A model of the V2R network type is considered in which one car in the cluster is defined as a central node that receives telematic information from other cars in the cluster and then transmits the collected information to the base station. It is proposed to replace the central vehicle with a specialized UAV that collects telematic information from all vehicles in the cluster and transmits the collected information to the base station. A variational optimization problem was compiled, the solution of which made it possible to determine the maximum amount of information that can be collected and transmitted from one cluster to the base station.

4 Conclusion

1. An information model of a cluster type for collecting and transmitting telematic information from one cluster has been constructed.
2. In relation to the V2R network model, it is proposed to replace the central vehicle of the cluster with a UAV, which performs the function of collecting and transmitting telematic information to the base station.
3. A formula has been obtained to calculate the maximum amount of information that can be collected and transmitted to the base station.

REFERENCES

- [1] M. Osinska, W. Zalewski, "Determinants of using telematics systems in road transport companies," *European Research Studies Journal*. Vol. XXIII. Iss. 2. 2020.
- [2] T. Zelinka, M. Svitek, Z. Lokaj, M. Srotyr, "Security of transport telematic solutions," *International journal of communications*. Iss. 4. Vol. 5. 2011.
- [3] Z. Xu, Q. Zhu, K.V. Prasad, "Data modeling and optimization for wireless drive-through applications," *Transaction on intelligent transportation systems*. Vol. 12. No 4. December 2011.
- [4] E. Hossain, G. Chow, V.C.M. Leung, B. McLeod, J. Mistic, V. Wong, O. Yang, "Vehicular telematics over heterogeneous wireless networks: A survey," *Computer communications*. 2010.
- [5] D. Jiang, L. Delgrossi, "Towards an international standard for wireless access in vehicular environments," *Proceedings of IEEE vehicular technology conference (VTC)*. May 2008, pp. 2036-2040.
- [6] Y. Lu, Y. Hong, C. Luo, D. Li, Z. Chen, "Optimization algorithms for UAV-and-MUV cooperative data collection in wireless sensor networks," *Drones* 2023. No. 7. P. 408. <https://doi.org/10.3390/drones7070408>.
- [7] X. Pang, J. Tang, N. Zhao, X. Zhang, Y. Qian, "Energy-efficient design for mm Wave-enabled NOMA-UAV networks," *Sci. China Inf. Sci.* 2021. No. 64, pp. 1-14. <https://doi.org/10.1007/s11432-020-2985-8>.
- [8] G. Gui, M. Liu, F. Tang, N. Kato, F. Adachi, "6G: opening new horizons for integration of comfort, security and intelligence," *IEEE Wirel. Commun.* 2020, pp. 126-132. <https://doi.org/10.1109/MWC.001.1900516>.
- [9] L.E. Elgolts, "Differential equations and calculus of variations," Moscow: Science. 1974. 432 p.

ANALYSIS OF METHODS TO INCREASE QOE PARAMETERS FOR VIDEO STREAMING SERVICES

Denis Chicherov ¹

¹ Institute of Radio and Information Systems (IRIS), Vienna, Austria; chicherovdenis@gmail.com

ABSTRACT

Video streaming services represent a new generation of television (DTV), which have become an integral part of modern digital culture. With the development of Internet technologies and the spread of broadband access, video streaming has become a popular and convenient way to consume multimedia content. Unlike traditional television, video streaming services provide the user with the ability to choose content, watch it at a convenient time and on different devices, which leads to new challenges and opportunities in improving the quality of user experience (QoE). One of the key elements that determine the quality of a video streaming service is the operator's transmission equipment and platform servers. These components provide content streaming over the Internet and affect such parameters as download speed, data stream stability and playback quality. Efficient management and optimization of the transmission equipment and servers can reduce latency, improve video quality and provide smoother streaming of content to end users. This research project aims to analyze methods for improving QoE parameters for video streaming services to better understand how technologies, algorithms and strategies can be applied to optimise the user experience in this new type of digital content. By considering factors such as video quality, adaptive streaming, traffic management, and many others, we aim to highlight key aspects that contribute to improving QoE and providing a more satisfactory user experience in video streaming services.

DOI: [10.36724/2664-066X-2024-10-2-28-36](https://doi.org/10.36724/2664-066X-2024-10-2-28-36)

Received: 10.02.2024

Accepted: 24.03.2024

Citation: Denis Chicherov, "Analysis of methods to increase QOE parameters for video streaming services," *Synchroinfo Journal* **2024**, vol. 10, no. 2, pp. 28-36.

Licensee IRIS, Vienna, Austria.

This article is an open access article distributed under the terms and conditions of the Creative Commons Attribution (CC BY) license (<https://creativecommons.org/licenses/by/4.0/>).



Copyright: © 2024 by the authors.

KEYWORDS: *Video streaming services, Digital television (DTV), Broadband access, Multimedia content consumption, User experience (QoE), Transmission equipment, Platform servers, Latency reduction, Adaptive streaming, Traffic management*

Analysing media streaming technologies

The process of live streaming is complex, involving numerous technologies that work in concert to produce the end result that viewers see when watching content. One technological aspect of this process is the delivery of video from the camera to the encoder, to the video host, and finally to the viewers. Professional broadcasters employ two main streaming protocols, MPEG-DASH and HLS, which are types of technology designed to transmit video files over the Internet.

In the past, online video was primarily delivered via the RTMP protocol. RTMP, or Real-Time Messaging Protocol, is a Flash-based video streaming standard that is still employed today to transmit video from an RTMP encoder to an online video platform. However, Flash-based video is no longer a viable option for delivering video to users. The Flash plug-in has lost value, and the number of devices supporting this outdated protocol is declining annually. It is no longer possible to run the Flash player in new versions of most web browsers. The RTMP protocol is gradually being replaced by the HLS protocol. In the last decade, the MPEG-DASH protocol has emerged as a competitor to HLS. It serves the same purpose as HLS, but because it is the newest variant, it is on the rise. This has led to a growing need to understand the difference between MPEG and HLS.

An overview of the comparison of these formats is presented in the table below (Table 1). Despite some advantages and merits neither MSS, HDS nor MPEG-DASH has been able to take as significant and dominant a role in the industry as Apple has done with its HLS.

In any case, the consumption of premium video content via online and mobile platforms has rapidly supplanted traditional television. The Internet has created a need for protocols to be developed to ensure high-quality images, depending on the device type and network congestion. Apple HLS, Microsoft Smooth Streaming and Adobe Flash HDS are adaptive delivery protocols that provide high-quality video consumption over the Internet.

Table 1

Comparison of different protocols

| Protocol name | DASH | HLS | MSS | HDS |
|----------------------------|--|---|----------------------------------|---------------------------|
| Type | Open, standards-based | Vendor-controlled | Vendor-controlled | Vendor-controlled |
| Video codecs | H.264 and other | H.264 | H.264, VC-1 | H.264, VP6 |
| Audio codecs | AAC and others | AAC, MP3 | AAC, WMA | AAC, MP3 |
| Fragment's format | MP4 и MPEG-2 TS | MPEG-2 TS | MP4 | MP4 |
| Files stored on the server | Adjacent or separate files per segment | Separate file per segment | Related | Related |
| Audio, video, text | Combined or chunked for audio and Video | Combined into one segment | Combined into one segment | Combined into one segment |
| Segmentation and delivery | Multiple vendors Standard HTTP or Broadcast server | Multiple vendors Standard HTTP or broadcast | MS IIS server (and a few others) | Adobe InteractiveServer |
| Playback | 3GPP-Rel 9 or MPEG clients | Apple iOS, QT X | Silverlight | Flash, Air |
| Security | Possibility to use third-party solutions | AES-128 | PlayReady | Flash Access |
| Segment length | Varies | 10 sec. | 2-4 sec. | 2-4 sec. |

Although one might expect that DASH is the most balanced and progressive protocol and therefore should be widely used, the reality is that it loses out due to greater complexity of implementation and patent issues. That said, HLS stands out due to its wide representation on a large number of mobile devices from its developer, and its ease

of implementation and ability to be used on other companies' devices makes it the most suitable at the moment. The MSS protocol has benefited from the success of the xbox range and well-known security systems. However, it is much more common in Europe than in America. HDS used to benefit from the ubiquity of Flash, but now that this technology is starting to move away, its future is highly debatable. To summarise, HLS is the undisputed market leader, although its competitors are in no hurry to give up so there may be some exciting competition in the future for media streaming technologies.

But it is also important not only to choose a media streaming technology, but also to implement the service itself correctly, because delays, adaptation, competent buffer handling are fundamental factors of quality server operation and user satisfaction, also known as QoE: Quality of Experience.

Comparing services that provide access to media content

As the viewing habits of consumers shift from traditional broadcasting to online streaming, the competitive landscape of online video is becoming increasingly intense. YouTube is now in its second decade on the global web, competing with its Vimeo-like counterparts or with other industry players such as Netflix. In the last five years, there have been some unsuccessful projects, as well as Amazon, the Seattle-based e-commerce giant known for its expansion into new markets, which is rapidly rising up the ranks to compete with industry titans such as Netflix.

A recent Internet usage report from Sandvine indicates that Amazon Video has become the third most popular online video service, trailing behind Netflix and YouTube. The network equipment company's biannual Global Internet Phenomena Report revealed that Amazon's streaming service now accounts for 4.3% of traffic during evening peak viewing hours.

Netflix continues to dominate the streaming video market, accounting for 35.2% of traffic in North America over the past year. Although this represents a slight decline from 37.1 per cent, the report notes that this is likely due to improvements in Netflix's video compression technology. However, measuring downstream Internet activity is not an exact metric, but it does provide insight into the usage of streaming services – a statistic that the services themselves are reluctant to provide.

Netflix was founded in 1997, with a total of approximately 65 million subscribers in 40 countries. In 2015, the company had over 100,000 pieces of content available for streaming. It is reported that 80% of sales come from recommendations. Netflix plays the role of a content 'aggregator'. However, in order to expand their business and increase their profits, they decided to produce their own content in addition to the usual video rental services [1].

Youtube (Google), founded in 2005, provides video streaming services over the Internet. Youtube is the largest provider of video streaming services, with an estimated 1.3 billion subscribers. In addition to providing video streaming services, Youtube offers video recommendations [2]. Amazon Prime Instant Video is a subscription-based video service, with a cost of \$99 per year. Amazon has extended its well-known book recommendation system to video.

It is evident that platforms differ not only in terms of design and subscription price, but also in terms of their underlying architecture. Each platform strives to ensure that the user can consume content in the most comfortable manner possible, as this is directly related to the user's satisfaction with the service. Consequently, the willingness of the user to pay for the service or to view advertisements on it is influenced. This, in turn, provides the owner of the media platform with the opportunity to earn money.

For example, according to the research [3] (Table 2) the average bitrate varies greatly from service to service depending on the codecs used, server settings and many other factors, which in turn has a significant impact on QoE.

Table 2

Average bitrate at different quality of transmitted picture on different multistreaming platforms [3]

| Platform | Bitrate 4K | Bitrate 1080p | Bitrate 720p |
|---------------------|------------|---------------|--------------|
| Apple TV + | 26 Mbps | 8,84 Mbps | 2,56 Mbps |
| Disney + | 16,59 Mbps | 7,42 Mbps | 4,42 Mbps |
| Netflix | 16,64 Mbps | 6,44 Mbps | 3,06 Mbps |
| Video premium | 10,02 Mbps | 5,12 Mbps | 3,18 Mbps |
| HBO | ND | 3,75 Mbps | 2,55 Mbps |
| The movie | ND | 4,13 Mbps | 2,57 Mbps |
| FlixOlé | ND | 6,66 Mbps | 2,68 Mbps |
| Atresplayer Premium | ND | 3,68 Mbps | 2,4 Mbps |
| RTVE Alacarta | ND | ND | 2,79 Mbps |
| Sky | ND | ND | 3,26 Mbps |
| FuboTV | ND | ND | 3,2 Mbps |

Client-based streaming for progressive loading

In order to apply the principle of streaming to progressive loading, servers, which have been controlling the loading up to this point, are replaced by clients that take over the streaming control and request video data from the servers. Clients only request data if their buffer is below a critical threshold. Once this threshold is exceeded, data is no longer requested. This limits the amount of video data that is wasted if playback is interrupted, and thus the amount of data that is wasted by the servers. This results in more efficient resource utilisation for the video service provider.

Client-based HTTP Adaptive Streaming: in order to be more flexible and avoid the need to evaluate the client's network conditions, the paradigm shift has evolved even further. Nowadays, video files are no longer stored as a whole file for each quality level (i.e. bitrate). Instead, they are stored as multiple files, so-called fragments or segments, each consisting of just a few seconds of playback time. The mapping of files to video segments is defined in a special media description file. This allows for a finer selection of quality (adaptive streaming). In combination with client-based streaming, an advantage arises because the client is directly aware of the current state of the network. This awareness encompasses the client's physical layer for data transmission and also includes the client's awareness of the video streaming capabilities due to the media description file. Consequently, client-based adaptive streaming can adapt seamlessly to changing network conditions by requesting video clips from the server at the appropriate bit rate. This results in the highest possible playback quality and reduced latency, which enhances the user experience [4]. Many proprietary solutions have implemented this new paradigm of client-based adaptive streaming. YouTube has also recently followed the current trend by integrating the standardised adaptive streaming technology MPEG Dynamic Streaming over HTTP (DASH) [5].

The popular Internet service YouTube has adopted Hypertext Markup Language Version 5 (HTML5) by default. This transition has resulted in YouTube adopting Dynamic Adaptive Streaming over HTTP (DASH) as its Adaptive Bit Rate (ABR) video streaming technology. Moreover, rate adaptation in DASH depends solely on the receiver. This problem motivated the authors of the paper [6] to perform an in-depth analysis (Figure 1 and 2) of a specific YouTube implementation of DASH. Firstly, this paper provides an overview of the state of the art in DASH and adaptive streaming technology and works related to the characterisation of YouTube traffic. Secondly, the paper describes a new methodology and testbed for traffic characterisation and performance measurement of

DASH implementation on YouTube. This methodology and testbed do not utilise proxies and are also capable of handling redirections of YouTube traffic.

Finally, a set of experimental results involving a dataset of 310 YouTube videos is presented. The presented results characterise YouTube traffic patterns and discuss the acceptable download bandwidth, the bitrate consumed by YouTube and the video quality. In addition, the results are cross-validated by analysing the HTTP requests made by the YouTube video player. The results of the paper [6] are applicable in the field of quality of service (QoS) and quality of experience (QoE) management. This is valuable information for Internet Service Providers (ISPs), as QoS management based on guaranteed downstream throughput can be used to ensure a targeted end-user quality of experience when using the YouTube service.

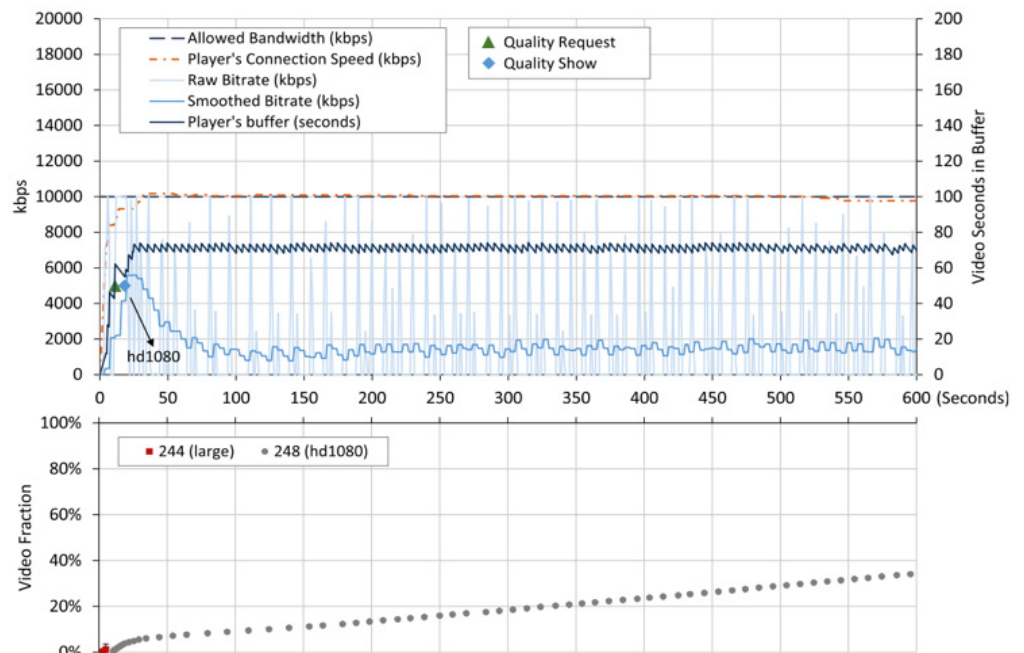


Figure 1. Test showing the bursting phase and throttling phase [6].

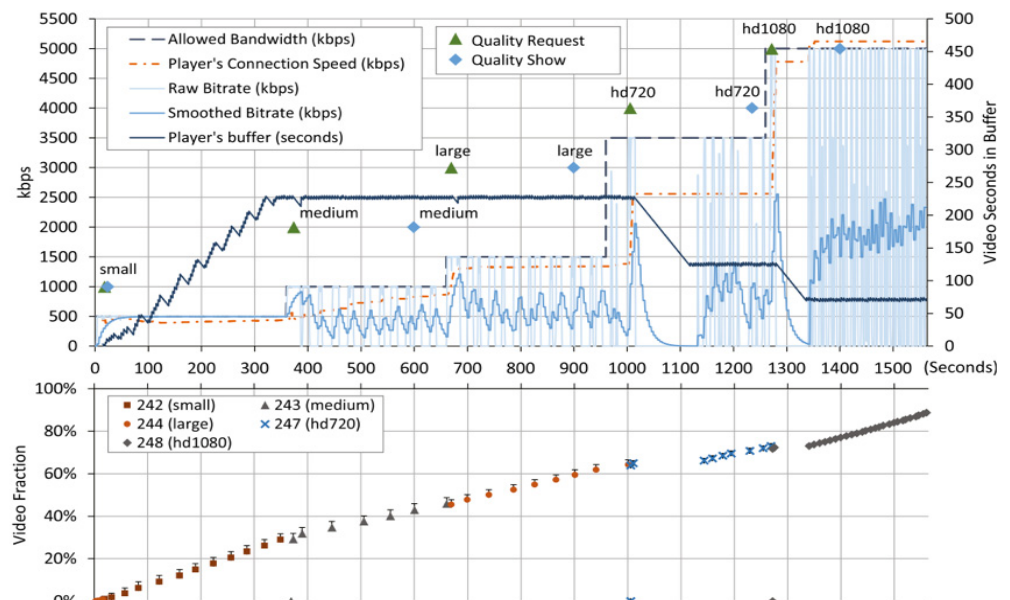


Figure 2. Test monotonically increasing scale of available download bandwidth [6].

As the description of the paper [7] suggests. This paper contributes to the existing literature by characterising the traffic of DASH implementations on YouTube and analysing YouTube's adaptation to dynamic conditions in terms of upload bandwidth fluctuations. In order to contribute, this paper firstly reviews the state of the art in DASH and adaptive streaming, and reviews related work on YouTube traffic analysis.

The proposed methodology and testbed included in this work allow us to characterise the structure of YouTube traffic without the use of proxy servers. In addition, the methodology and testbed address the problem of YouTube redirections, which has been pointed out in other papers [8]. A large dataset of 310 videos was used for the presented tests. In these tests, network parameters, internal YouTube player parameters and HTTP requests of the YouTube player were correlated. Moreover, a number of experimental results were obtained showing interesting results. The average YouTube download bitrate was obtained, capturing the requested quality, but it was shown that it was not useful for making bandwidth provisioning decisions. Instead, information was provided on the required available bandwidth to obtain a certain requested quality automatically with an estimated probability. It is also observed that the video bitrate requirements on the quality level of YouTube videos have increased compared to the results obtained in [9] in 2015.

Optimising video streaming parameters to improve user satisfaction

Video quality and resolution:

Investigating the impact of video resolution on user satisfaction is a key aspect in QoE optimisation. The optimal resolution depends on many factors, such as the type of content and the device on which it is viewed. For example, for static content such as films or TV series, a high resolution may be preferred to provide a more immersive content experience. However, for dynamic content, such as video games or sports broadcasts, a lower resolution with a higher frame rate may be preferred to reduce latency and provide smooth playback.

Adaptive streaming:

Adaptive streaming is a technique that optimises playback quality depending on the available bandwidth and the characteristics of the user's device. Adaptive streaming algorithms automatically select the optimal video resolution and bitrate for each particular moment in time, based on the current network and user device conditions. This allows for the best possible playback quality to be provided to the user while minimising latency and interruptions [10].

Latency and buffering:

Latency and buffering can have a significant impact on QoE, as they can cause playback interruptions and degrade the overall user experience when viewing content. Intermittent stops or long delays in video loading can cause annoyance and degrade user satisfaction [11].

Exploring methods to reduce latency and optimise buffering plays an important role in improving QoE. One approach could be the use of data preloading algorithms or buffering optimisation combined with adaptive streaming. This can reduce latency and provide smoother content playback, which ultimately contributes to increased user satisfaction.

Traffic management and network protocols:

Studying the impact of network protocols such as HTTP, UDP on streaming video quality and the possibility of optimising them represents a significant research area. Different protocols have different transmission characteristics that can significantly affect QoE. For example, HTTP is often used for video transmission over the Internet, but can cause delays and quality degradation in case of unstable connection. Investigating the performance of different network protocols and developing methods to optimise them will help improve video streaming quality and overall user satisfaction.

Audio Quality:

Conducting research on the impact of audio quality on overall user satisfaction and how it can be improved is an important aspect of optimising QoE in video streaming services. While attention is often focused on video quality, audio quality is also important to the user experience. Exploring methods to improve audio quality, such as audio compression technologies or the use of high-quality audio codecs, can help create a more enjoyable and engaging user experience.

Personalised content:

Exploring methods of delivering personalised content and its impact on QoE is an important aspect of the development of video streaming services. Personalising content allows users' individual preferences and interests to be taken into account, which can significantly improve their satisfaction and time spent on the platform. Exploring methods of audience segmentation, user behaviour analysis and recommendation systems will help to develop effective strategies to deliver personalised content and optimise QoE for each user.

QoE evaluation metrics:

Developing or analysing metrics to evaluate QoE is a key aspect in video streaming. Effective metrics should consider various aspects of the user experience, including video and audio quality, playback latency, and interface usability and content availability. Conducting a study to develop such metrics will help improve the ability to conduct service quality assessments and identify areas for improvement.

Impact of devices and platforms:

Examining the differences in QoE across devices and platforms is an important aspect of the study. Users may use different devices, such as computers, smartphones or smart TVs, with different operating systems such as iOS, Android or Windows. Each of these platforms may present unique technical and user characteristics that affect QoE. Exploring these differences will help to develop optimisation strategies for different platforms and devices to ensure consistent playback quality for all users.

Cloud Computing and Distributed Systems:

Exploring the potential of cloud computing and distributed systems in the context of improving QoE in video streaming represents an important research direction. Cloud computing can provide scalability and flexibility for processing and storing multimedia data and for delivering content to end users. Distributed systems can improve the availability and reliability of video streaming services by providing data backup and query processing closer to end users. Research into these technologies can lead to the development of more efficient and reliable video streaming services [12].

Machine Learning and Data Analytics:

The application of machine learning and data analytics to optimise QoE parameters is a promising area of research. Machine learning can be used to predict user preferences, identify anomalies in the data stream, and automatically adjust playback parameters for each user. Data analysis can help identify patterns and trends in user behaviour, which can help optimise video quality, traffic management and other aspects of video streaming services [13-14].

Summary and Conclusion:

In this chapter, various aspects of optimising QoE parameters for video streaming services have been discussed. The study has shown that video quality and resolution play a key role in user satisfaction and the optimal parameters may vary depending on the type of content and user devices.

Adaptive streaming allows dynamic adaptation of playback quality based on network and device conditions, which significantly improves the viewing experience and user satisfaction.

Latency and buffering have a direct impact on QoE, and optimising these parameters can significantly improve user satisfaction and reduce the likelihood of churn.

Traffic management and choice of network protocols are also important to ensure stable and high-quality video content playback.

Audio quality and personalised content are additional aspects that can significantly improve user experience and satisfaction.

Thus, to ensure a high level of QoE in video streaming services, it is necessary to take a comprehensive approach that takes into account all of these aspects and optimises each of them based on user needs and preferences.

Optimising operator transmission equipment to improve QoE

Operator transmission equipment plays a key role in delivering content from the provider to the end user. Optimising this equipment can significantly improve user satisfaction and quality of user experience (QoE). Below are some ways that can help in improving QoE through optimising the operator's transmission equipment:

1. Increase network bandwidth: Ensuring sufficient network bandwidth allows video content to be transmitted at higher resolution and quality. This can be achieved through upgrading network equipment, increasing link bandwidth and optimising traffic routing.

2. Deployment of caching servers: Placing caching servers closer to end users reduces latency and content download time. This improves user experience, especially for streaming services with high traffic volumes.

3 Using CDN technology: Content delivery networks (CDNs) allow content to be distributed to different nodes in the network, reducing the distance and time it takes to deliver content to the end user. This reduces network load and improves QoE by increasing download speeds and reducing playback latency.

4. Monitoring and Quality of Service (QoS) Management: Implementing QoS monitoring and management systems allows operators to monitor network performance and respond to potential problems before they occur. This helps prevent playback interruptions and ensures stable, high-quality content playback.

5. Optimised data encoding and compression: Using advanced data encoding and compression techniques, content can be delivered with higher quality at lower bandwidths. This reduces network resource utilisation and improves QoE for users with limited access to broadband.

These techniques can help operators optimise transmission equipment and improve QoE for users of video streaming services. By investing in state-of-the-art equipment, utilising advanced technologies and network management, operators can ensure stable and high-quality content playback, leading to higher user satisfaction and increasing the competitiveness of their services in the market.

Conclusion

In today's world, video streaming services have become an integral part of our lives, providing access to a variety of media content anytime and anywhere. In this study, we have examined several key aspects of media streaming technologies and optimising parameters to improve user satisfaction (QoE).

Analysing media streaming technologies allowed us to familiarise ourselves with the main methods of delivering content to end-users and to understand which technologies are the most effective in terms of user satisfaction.

We looked at comparing different services that provide access to media content, which allowed us to understand their strengths and weaknesses.

Optimising video streaming parameters to improve user satisfaction was the central theme of our research. We looked at the impact of video resolution, adaptive streaming, latency and buffering, traffic management and network protocols, audio quality, personalised content, QoE evaluation metrics, device and platform impact, cloud computing and distributed systems, machine learning and data analytics on overall user satisfaction.

We concluded the study by highlighting the importance of optimising an operator's transmission equipment to improve QoE. This means that operators should invest in state-of-the-art equipment, utilise advanced technologies and manage the network in a way that ensures stable and high quality content playback for their users.

Thus, our research allowed us to cover a wide range of topics related to video streaming services and identify the key factors that affect user satisfaction. The implementation of the proposed recommendations will help operators and providers to achieve a high level of QoE and strengthen their positions in the media streaming market.

REFERENCES

- [1] Xavier Amatrain and Justin Basilico, "Netflix recommendations: beyond the 5 stars (part 1), Netflix Tech Blog," <http://techblog.netflix.com/2012/04/netflix-recommendations-beyond-5-stars.html>, 2012.
- [2] D. James, L. Benjamin, "The YouTube Video Recommendation System," *RecSys '10 Proceedings of the fourth ACM conference on Recommender systems*, pp. 293-296, Sep 2010.
- [3] <https://samagame.com/blog/en/which-streaming-service-has-better-picture-quality-we-compare-netflix-hbo-disney-prime-video-and-seven-other-platforms/>
- [4] J. Yao, S. S. Kanhere, I. Hossain, and M. Hassan, "Empirical evaluation of HTTP adaptive streaming under vehicular mobility," *Networking*. Springer, 2011, pp. 92-105.
- [5] 'ISO/IEC 23009-1:2012 information technology – dynamic adaptive streaming over HTTP (DASH) – part 1: Media presentation description and segment formats,' 2012.
- [6] Javier Añorga, Saioa Arrizabalaga, Beatriz Sedano, Jon Goya, Maykel Alonso-Arce, Jaizki Mendizabal. Analysis of YouTube's traffic adaptation to dynamic environments.
- [7] Candid with YouTube: Adaptive Streaming Behavior and Implications on Data Consumption.
- [8] L. Plissonneau, E. Biersack, P. Juluri, "Analyzing the impact of YouTube delivery policies on user experience," *Proceedings of the 24th international Teletraffic congress*, 2012, p. 28.
- [9] J. Añorga, S. Arrizabalaga, B. Sedano, M. Alonso-Arce, J. Mendizabal, "YouTube's DASH implementation analysis," *19th International Conference on Circuits, Systems, Communications and Computers, (CSCC 2015)*, July 16-20, 2015, Zakynthos Island, Greece.
- [10] Y. Chao, X. Jimin, Z. Yao and M. Anlong, "Video streaming adaptation strategy for multiview navigation over DASH," *IEEE Trans. Broadcast.*, vol. 65, no. 3, pp. 521-533, Sep. 2019.
- [11] Jewon Lee, Eunhee Hyun, Soon-Choul Kim, Joon-Young Jung, "A Viewport Adaptive Low-latency Streaming System for Large-scale Multi-view Service," *2023 14th International Conference on Information and Communication Technology Convergence (ICTC)*.
- [12] Design of Distributed Network Mass Data Processing System Based on Cloud Computing Technology Fanghai Gong 2021 Fifth International Conference on I-SMAC (IoT in Social, Mobile, Analytics and Cloud) (I-SMAC).
- [13] Mahmoud Darwich, Kasem Khalil, Magdy Bayoumi, "Smart Streaming: Deep Learning Applications in Video Streaming Optimization", *SoutheastCon 2024*, pp. 22-27, 2024.
- [14] Mahmoud Darwich, Kasem Khalil, Magdy Bayoumi, "Optimizing QoE in IoT-Based Video Streaming through Deep Learning Algorithms", *2024 International Conference on Artificial Intelligence in Information and Communication (ICAIIIC)*, pp. 052-057, 2024.

PEAK-TO-AVERAGE POWER RATIO OF SPECTRALLY EFFICIENT FDM SIGNALS

Ngok Nuen Tan ¹,

¹ Vietnam National University – Ho Chi Minh, Ho Chi Minh City, Vietnam

ABSTRACT

The change of the number of subcarriers in SEFDM signal from 5 to 1024 leads to the growth of the PAPR (peak-to-average power ratio) from 4.5 to 9 dB. PAPR of SEFDM signals stays about constant (instability is no more than 5%) while normalized subcarriers frequency spacing increase from 1/2 to 1. It indicates no additional energy loss during the transition from OFDM signals to SEFDM signals, caused by an increase in the PAPR. It is proposed to use a part of the resulting gain in the frequency band to reduce PAPR. The method, based on modification of Tone Insertion method, was developed. Developed method consists in adding additional subcarriers with randomly generated manipulation symbols to the SEFDM signal. SEFDM symbol with minimal PAPR is chosen to be send. According to this method the PAPR can be reduced in average of 1.4 dB. The degree of reduction of the PAPR depends on the size of the channel alphabet of additional subcarriers (changing of the average win is 0.6 dB for BPSK to 1.4 dB for QAM-64) and the number of combinations of symbols of additional subcarriers (1.6 dB for 1000 combinations for QAM-64). According to estimation of the FPGA resources for implementation of PAPR reduction algorithm it is required relatively small resource costs compared to the formation of SEFDM signal without reduction.

KEYWORDS: *telematics, cluster, UAV, drones, optimization, information collection, base station.*

DOI: [10.36724/2664-066X-2024-10-2-37-43](https://doi.org/10.36724/2664-066X-2024-10-2-37-43)

Received: 15.02.2024

Accepted: 20.03.2024

Citation: Ngok Nuen Tan, "Peak-to-average power ratio of spectrally efficient FDM signals," *Synchroinfo Journal* **2024**, vol. 10, no. 2, pp. 37-43

Licensee IRIS, Vienna, Austria.

This article is an open access article distributed under the terms and conditions of the Creative Commons Attribution (CC BY) license (<https://creativecommons.org/licenses/by/4.0/>).



Copyright: © 2024 by the authors.

1 Introduction

Orthogonal frequency division multiplexing (OFDM) signals are widely used in systems such as Wi-Fi, WiMAX, LTE, DVB-T2, DAB, DRM and 4G LTE downlink [1, 2]. Currently, active research is underway on signal systems for fifth generation communication networks. Multi-frequency signals with non-orthogonal multiplexing (Spectrally Efficient FDM signals) are considered as the most promising alternative to OFDM in these networks. Such signals are formed from OFDM signals by reducing the spacing between subcarriers, thereby significantly increasing the spectral efficiency of the signals [11, 12].

The main disadvantage of multi-frequency signals is the high peak factor and, as a consequence, significant underutilization of output amplifiers in terms of power [2, 5]. In portable transceiver devices, a high peak factor value (5-10 dB) causes a limitation in the signal amplitude at the transmitter output and, as a consequence, an increase in the level of out-of-band emissions [6]. The peak factor of OFDM signals has been well studied today [13-15], and a large number of different methods have been proposed to reduce it [7, 8]. However, the issue of reducing the peak factor of SEFDM signals has been poorly considered. In this work, an algorithm for reducing the peak factor is developed, based on a modification of the Tone Insertion method [9]. The developed algorithm makes it possible to reduce the peak factor by an average of 1.5 dB for the case of 103 subcarriers at moderate costs for its implementation.

The goal of the work is to reduce the peak factor of SEFDM signals.

To achieve this goal, the following tasks were solved in the work:

1. assessment of mathematical expectations and variances of the peak factor of SEFDM signals for the number of subcarriers used from 5 to 32768, various manipulation methods and compression factors;
2. construction of integral distribution functions for the peak factor of SEFDM signals;
1. analysis of existing algorithms for reducing the peak factor and proposing an option for reducing it for a large number of subcarriers;
2. assessment of the feasibility of the proposed algorithm for reducing the peak factor in programmable logic integrated circuits (FPGA).

2 Generation of SEFDM signals. Peak factor

The main characteristic of SEFDM signals is the compression factor:

$\alpha = \Delta f T = \Delta f / \Delta f_{\text{opt}}$, where Δf_{opt} – Frequency domain subcarrier spacing for

orthogonal signals. For OFDM signals $\alpha = 1$. SEFDM signals occupy less bandwidth than OFDM signals, i.e. for $\Delta f < \Delta f_{\text{opt}}$ compaction factor $\alpha < 1$.

For a finite discrete signal $s_N(i)$, corresponding to the n th FDM symbol, extended in duration to N samples, the following expression is satisfied:

$$s_N(i) = \frac{1}{N} \sum_{k=0}^{N-1} C_N(k) e^{j2\pi \frac{ki}{N}}, \quad i = 0, \dots, (N-1),$$

where $C_{N(k)}$ – manipulation symbols (index N indicates the duration of the symbol). The signal is generated by an N -point inverse discrete Fourier transform (IDFT) from the manipulation symbols $C_{N(k)}$, after which the sequence of samples of length N obtained at the output of the IDFT is truncated to L samples [3].

The peak factor P of a SEFDM signal will be the ratio of the highest (peak) power to the average power P_{cp} of the signal $s(t)$ for the duration of one symbol T :

$$P = \frac{\max_{t \in [0; T]} \{|s(t)|^2\}}{P_{cp}}, P_{cp} = \frac{1}{T} \int_0^T |s(t)|^2 dt.$$

Note that the peak factor of SEFDM signal is a random variable.

3 Peak factor analysis of SEFDM signals

To analyze the peak factor of SEFDM signals, two approaches to generating SEFDM words were used: for all possible variants of manipulation symbols and for randomly generated manipulation symbols. The second approach was used to analyze the peak factor of signals with the number of subcarriers greater than 15, or the volume of the channel alphabet greater than 16.

The obtained quantitative results of the oscillation peak factor for 5 and 1024 subcarriers for two keying methods (FM-2 and QAM-64) and compression factors α : 1/2, 3/4, 7/8, 15/16, 1 are presented in Table 1. Columns $E_{\alpha, N(s)}$ show the values of the peak factor of the random SEFDM signal s averaged over the entire ensemble of implementations. Here $E_{\alpha, N(s)}$ is the mathematical expectation of signal s , depending on both α and the number of subcarriers N , the manipulation method and the number of implementations. Values for 1024 subcarriers are given for 106 implementations.

Table 1

Quantitative results of peak factor changes

| | | |
|--------|------|------|
| FM-2 | 0,50 | 2,62 |
| | 0,75 | 2,70 |
| | 0,88 | 2,70 |
| | 0,94 | 2,67 |
| | 1,00 | 2,63 |
| QAM-64 | 0,50 | 2,38 |
| | 0,75 | 2,73 |
| | 0,88 | 2,87 |
| | 0,94 | 2,87 |
| | 1,00 | 2,87 |

From Table 1 it can be seen that with an increase in the number of subcarriers, there is an increase of approximately 2.5 times (from 4.5 to 9 dB) in the peak factor values averaged over the ensemble of SEFDM signals, which practically do not change when moving from one value of the compression factor to another.

By calculating the peak factor of the corresponding SEFDM symbol for each information word and sorting the obtained results in ascending order and representing them as a column vector, it is possible to obtain the dependence of the peak factor of the SEFDM signal on the serial number in the column vector. The resulting distribution for the case $\alpha = 3/4$ is presented in Figure 1.

Figure 2 shows the integral distribution functions for four manipulation methods. On it, the average values of the peak factor over the ensemble of SEFDM signals are plotted

along the abscissa axis, and the values of the integral distribution function of the peak factor $F(\Pi)$ are plotted along the ordinate axis. From Figure 2 it can be seen that the integral distribution functions for QAM-16 and QAM-64 practically coincide, which is due to the large number of combinations of manipulation symbols.

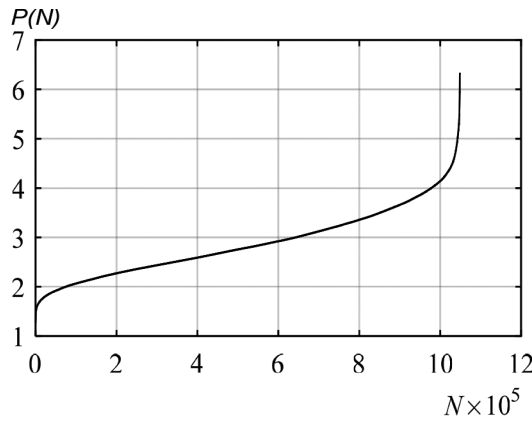


Fig. 1. Dependence of the peak factor of a SEFDM signal on the serial number in the vector-column vector for a signal with QAM-16, 5 subcarriers and $\alpha = 3/4$

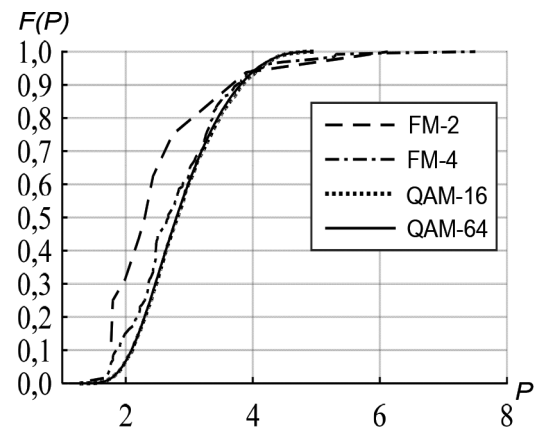


Fig. 2. Cumulative distribution functions of the SEFDM signal peak factor

4 Peak factor reduction algorithm

To reduce the peak factor of SEFDM signals, an algorithm based on the Tone Insertion method was developed [9]. The essence of the algorithm is as follows: additional subcarriers are added to the original signal (SEFDM symbol), the complex amplitudes of which are selected in such a way as to reduce the peak factor of the original signal. The developed algorithm alternates information subcarriers with additional subcarriers. In this case, the occupied frequency band becomes wider depending on the number of additional subcarriers.

The Tone Insertion method is presented in Figure 3a, its proposed modification is shown in Figure 3b. The abscissa axis shows the frequency domain, the ordinate axis shows a schematic representation of frequency subcarriers (dashed lines show additional subcarriers).

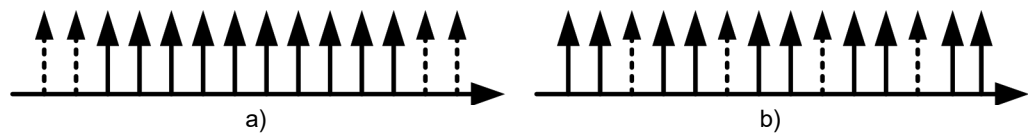


Fig. 3. Methods for adding additional subcarriers: a) along the edges of the used subcarriers (Tone Insertion); b) alternating used and additional subcarriers

Both methods, with similar parameters, provide the same reduction in peak factor on average. However, when constructing a distribution histogram and its bicubic approximation, one can see a wider spread in the ratio of the original peak factor of the SEFDM signal to the maximum possible reduction in the peak factor over the symbol duration for the second approach.

The specified spread of peak factor values is presented in Figure 4, in which the x-axis shows the ratio of the original peak factor of the SEFDM signal to the maximum possible reduction in the peak factor over the duration of the symbol, which we will call gain, and the ordinate axis shows the normalized number of sample elements. In this case, normalization is necessary due to the different widths of the pockets of the original distribution histogram (for the second method, the distribution histogram without normalization is approximately twice as high).

The gain is calculated by finding the ratio of the peak factor of the SEFDM signal before reduction (P_{orig}) in the absence of additional subcarriers to the peak factor of the SEFDM signal after adding additional subcarriers (P_s). To each information vector, presented as points on the complex plane, elements of an additional vector are added, the elements of which are formed randomly according to a uniform distribution. After that, SEFDM signals are generated in the time domain and the peak factor is calculated for each implementation of the additional vector. After calculating the peak factors for all implementations of the additional vector, the SEFDM symbol with the minimum peak factor is selected to be sent to the channel.

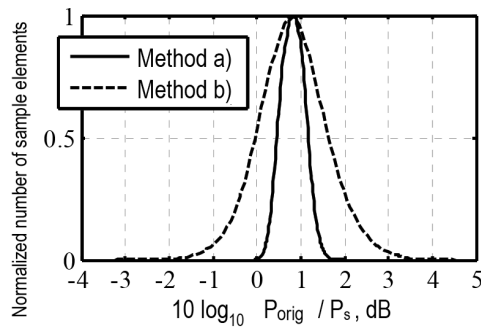


Fig. 4. Normalized bicubic approximation of the histogram of the peak factor gain distribution for 105 information vectors and 100 combinations of additional subcarriers (FM-4 for the used subcarriers, $\alpha = 3/4$, FM-4 for 32 additional subcarriers)

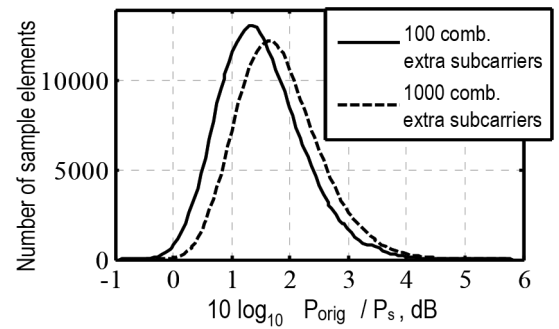


Fig. 5. Bicubic approximations of the distribution histograms of the peak factor gain depending on the number of combinations of additional subcarriers for 105 information vectors (FM-4 for the used subcarriers, $\alpha = 3/4$, QAM-64 for 32 additional subcarriers)

Obviously, the more SEFDM symbols with different combinations of additional subcarriers are generated, the greater the reduction in peak factor can be obtained. Figure 5 shows bicubic approximations of the distribution histograms of the peak factor gain depending on the number of combinations of additional subcarriers for 105 information vectors.

In the course of studying the influence of the method of manipulating additional subcarriers on the peak factor, it was found that the gain increases with increasing volume of the alphabet of the signal constellation (Fig. 6). Based on Figure 6, the change in the average gain ranges from 0.6 dB for FM-2 to 1.4 dB for QAM-64.

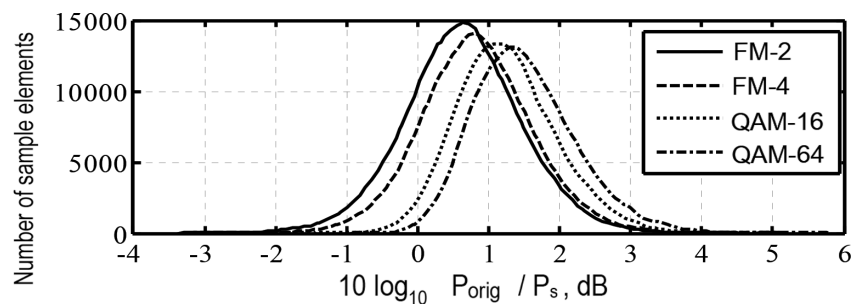


Fig. 6. Bicubic approximations of the distribution histograms of the peak factor gain depending on the method of manipulation of additional subcarriers for 105 information vectors (FM-4 for the subcarriers used, $\alpha = 3/4$, 100 combinations of 32 additional subcarriers)

5 Implementation proposals

Inverse Fast Fourier transform – (IFFT) from a vector decimated by zeros with information elements at M_k positions ($k = 0, \dots, M$, where $M - 1$ is the number of information elements between zero positions) is equal to the IFFT of dimension M repeated N_{fft}/M times without decimation, where N_{fft} is the dimension of the OBFT. In addition, when a zero appears at any of the M_k positions, a zero appears at the k -th position of the OBFT of dimension M . The latter property is used when adding additional subcarriers in the case of using guard intervals in the frequency domain.

The advantage of the second method over the first is the ability to use blocks (Inverse Discrete Fourier Transform – IDFT) of a smaller dimension than the main ODFT block to form SEFDM symbols from combinations of additional subcarriers. An example of interleaving for 12 information subcarriers and four additional subcarriers is presented in Figure 7a. Thus, it will be necessary to create a zero-decimated OFDM symbol once, as shown in Figure 7b, and then transition to a SEFDM symbol.

The symbols of additional subcarriers form an IFFT of dimension M (in the example in Figure 7c ($M = 4$, $N_{\text{fft}} = 16$), and the resulting vector is sequentially duplicated N_{fft}/M times, after which it is converted according to the rule for generating SEFDM symbols and added to the previously generated SEFDM symbol. This happens a predetermined number of times for various combinations of additional subcarrier keying symbols, after which the peak factor is calculated and the SEFDM symbol with its minimum value is selected.

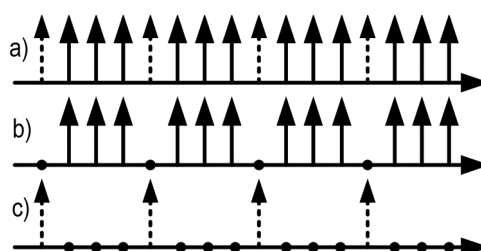


Fig. 7. Example of interleaving for 12 information subcarriers and four additional subcarriers: a) information vector in the frequency domain with additional subcarriers; b) information vector decimated by zeros; c) presentation of additional subcarriers

The proposed method for reducing the peak factor can be implemented using FPGA. To generate one reduced peak factor SEFDM symbol for a WiMAX communication system, one 1024-point IFFT and 100 32-point IFFTs are required. Considering that the latency of a 1024-point OBPF on the Xilinx board of the Virtex 7 family is 2171 clock cycles (or 8.684 μ s), and the latency of a 32-point OBPF is 142 clock cycles (or 0.568 μ s) [10], then in one formation of zero-decimated information vectors can be made sequentially in one 32-point block of $2171/142 \approx 15$ pseudo-random combinations of additional subcarriers. The number of pseudo-random combinations increases according to the increase in the number of parallel installed 32-point IFFT blocks as $15k$, where k is the number of 32-point IFFT blocks.

5 Conclusion

When changing the number of subcarriers in a SEFDM signal from 5 to 1024, the average peak factor increases from 4.5 to 9 dB. The peak factor of SEFDM signals practically did not change (no more than 5%) with an increase in the frequency multiplexing factor from 1/2 to 1, which indicates the absence of additional energy loss when moving from orthogonal to non-orthogonal signals due to an increase in the peak factor.

To reduce the peak factor, it is proposed to use part of the resulting gain in the occupied frequency band. The developed modification of the Tone Insertion method, which consists in adding additional subcarriers with various combinations of keying symbols, allows reducing the peak factor by an average of 1.4 dB. The degree of reduction in the

peak factor depends on the volume of the channel alphabet of additional subcarriers (the change in the average gain value ranges from 0.6 dB for FM-2 to 1.4 dB for QAM-64), as well as on the number of iterations of symbol combinations on additional subcarriers (1.6 dB for 1000 searches for QAM-64).

According to the above assessment of the used FPGA resources, implementing the peak factor reduction algorithm will require relatively small additional resource costs compared to generating a SEFDM signal without reducing it.

REFERENCES

- [1] IEEE Standard for Wireless MAN-Advanced Air Interface for Broadband Wireless Access Systems, IEEE Standard 802.16.1, 2012.
- [2] V.M. Vishnevsky, A.I. Lyakhov, S.L. Portnoy, I.V. Shakhnovich, "Broadband wireless information transmission networks," Moscow: Technosphere, 2005, 592 p.
- [3] A.B. Kisliitsyn, A.V. Rashich, Ngok Nuen Tan, "Generation of SEFDM-Signals Using FFT/IFFT," *14th International Conference, NEW2AN 2014 and 7th Conference, ruSMART 2014*, Proceedings, 8638 LNCS, pp. 488-501 (http://link.springer.com/chapter/10.1007%2F978-3-319-10353-2_44).
- [4] K.A. Chorti, M. Rodrigues, I. Darwazeh, "Analysis of Sub-optimum detection techniques for a bandwidth efficient multi-carrier communication system," *Proceedings of the Cranfield Multi-Strand Conference*, Cranfield University, pp. 505-510, May 2009.
- [5] L. Wang, C. Tellambura, "An Overview of peak-to-average power ratio reduction techniques for OFDM systems," *Signal Processing and Information Technology, 2006 IEEE International Symposium*, Aug. 2006, pp. 840-845.
- [6] S.B. Makarov, I.A. Tsikin, "Transmission of discrete messages over radio channels with limited bandwidth," Moscow: Radio and communications, 1988. 304 p.
- [7] L. Wang, C. Tellambura, "An Overview of peak-to-average power ratio reduction techniques for OFDM systems," *Signal Processing and Information Technology, 2006 IEEE International Symposium*, Aug. 2006, pp. 840-845.
- [8] S.H. Han, J.H. Lee, "An Overview of peak-to-average power ratio reduction techniques for multicarrier transmission," *IEEE Wireless Communications*, April 2005.
- [9] IEEE Dummy tone insertion for spectral sculpting of the multi-band OFDM UWB system (<http://ieeexplore.ieee.org/xpl/login.jsp?tp=&arnumber=4808854&url=http%3A%2F%2Fieeexplore.ieee.org%2Fiel5%2F4799765%2F4808829%2F04808854.pdf%3Farnumber%3D4808854>)
- [10] Xilinx LogiCORE IPFast Fourier Transform v8.0 (http://www.xilinx.com/support/documentation/ip_documentation/ds808_xfft.pdf)
- [11] X. Liu, X. Liu, M. Jia, F. Li and T. S. Durrani, "Simultaneous Wireless Information and Power Transfer Based on Time-Frequency Block Allocation in OFDM Cooperative Communication System," *IEEE Systems Journal*, vol. 16, no. 3, pp. 4827-4830, Sept. 2022, doi: 10.1109/JSYST.2021.3093572.
- [12] Y. Xiang, Y. Gao, X. Yang, S. Kang and M. Shao, "An ESPRIT-Based Moving Target Sensing Method for MIMO-OFDM ISAC Systems," *IEEE Communications Letters*, vol. 27, no. 12, pp. 3205-3209, Dec. 2023, doi: 10.1109/LCOMM.2023.3325531.
- [13] W -W. Hu, "Enhanced Performance of Asymmetrically Clipped DC-Biased Optical OFDM Systems Using Adjacent Symbol Detection," *IEEE Photonics Journal*, vol. 15, no. 6, pp. 1-7, Dec. 2023, Art no. 7304607, doi: 10.1109/JPHOT.2023.3324368.
- [14] Y. Sun and H. Ochiai, "Maximum-Likelihood-Based Performance Enhancement of Clipped and Filtered OFDM Systems With Clipping Noise Cancellation," *IEEE Wireless Communications Letters*, vol. 11, no. 3, pp. 448-452, March 2022, doi: 10.1109/LWC.2021.3131313.
- [15] K. Zheng and X. Ma, "Secure OFDM Transmissions With Coset-QAM," *IEEE Wireless Communications Letters*, vol. 13, no. 3, pp. 824-828, March 2024, doi: 10.1109/LWC.2023.3346288.

NONCOHERENT DATA TRANSFER BY USING ORTHOGONAL NOISE SIGNALS

Liu Wenkui ¹,

¹ Nanjing university of science and technology, Jiangsu, China

ABSTRACT

The modern period of communications development is associated with the search and use of new broadband noise-like signals. One of the pressing problems in this area – large-power ensembles synthesis of broadband noise-like signals with good correlation and group properties. Another problem is the difficulty of isolating components from a mixture of several broadband noise-like signals under noise conditions, as well as the difficulty of reproducing such signals during correlation reception shape. The article discusses an incoherent correlation method of data transmission, based on the use of signals generated on the transmitter side by some noise generator. The noise signal is divided into parts (noise pulses) of a given duration. When the current noise pulse is transmitted, the next noise pulse is orthogonalized or collinearized depending on the transmitted data bit. On the receiver side, the mutual energy of the current and previous noise pulse is calculated. If this energy is less than the threshold, a decision is made to transmit zero, otherwise, to transmit one. Synchronization of the receiver and transmitter is carried out by changing the sign of the mutual energy of adjacent noise pulses.

DOI: [10.36724/2664-066X-2024-10-2-44-50](https://doi.org/10.36724/2664-066X-2024-10-2-44-50)

Received: 25.03.2024

Accepted: 10.04.2024

Citation: Liu Wenkui, "Noncoherent data transfer by using orthogonal noise signals," *Synchroinfo Journal* 2024, vol. 10, no. 2, pp. 44-50

Licensee IRIS, Vienna, Austria.

This article is an open access article distributed under the terms and conditions of the Creative Commons Attribution (CC BY) license (<https://creativecommons.org/licenses/by/4.0/>).



Copyright: © 2024 by the authors.

KEYWORDS: *noncoherent data transfer, orthogonal noise signals, synchronization, receiver, transmitter.*

1 Introduction

The noncoherent communication systems based on the using of orthogonal noise signals is discussed. The noise signal is divided into pulses noise of the given duration T . When transmitting current pulse γ_i next pulse γ_{i+1} exposed orthogonalization or collinearization depending on each bit of data $\rho_i \in \{-1, +1\}$:

To synchronize transmitter and receiver is used a change of sign of mutual energy of the neighboring pulses [1-4, 8].

On the receiver side it is calculated the scalar product the current γ_{i+1} and previous received pulse noise γ_i . If the scalar product module is less than the threshold ε the transfer of zero is detected, otherwise, the transfer of unit is detected:

Receiver and transmitter synchronization is based on the identification of energy integral derivative gap when changing from one pulse noise to another:

$$t_i : \left| \frac{d}{dt} \left(\int_0^{T+\Delta T} \gamma_i(t) \times \gamma_{i+1}(t) dt \right) \right| = \pm \Delta \quad (i = \overline{1, N}),$$

where t_i – moment of the end of the pulse noise γ_i , ΔT – maximum synchronization error, ε – the threshold of clock signal. The proposed method allows achieving an arbitrarily small error probability by one bit.

2 Noise signals orthogonalization

Let noise pulses of duration T be given

$$\chi_i(t) (i = \overline{0, N}, t \in [0, T]), \tag{1}$$

received from some noise generator. Define a vector space in which the operations of adding signals [5], multiplying a signal by a constant and scalar product are specified:

$$\begin{aligned} z &= x + y, \quad z(t) = x(t) + y(t) \quad (t \in [0, T]); \\ z &= \alpha x, \quad z(t) = \alpha \times x(t) \quad (t \in [0, T]); \\ (x, y) &= \int_0^T x(t) \times y(t) dt, \end{aligned}$$

where operations on numbers are performed in some finite or infinite field F .

Perform Gram-Schmidt orthogonalization procedures for signals (1):

$$\gamma_i = \chi_i - \sum_{j=0}^{i-1} \frac{(\chi_i, \chi_j)}{(\chi_j, \chi_j)} \chi_j \quad (i = \overline{0, N}). \tag{2}$$

As a result, we obtain orthogonal noise signals (2) such that

$$\int_0^T \gamma_i(t) \times \gamma_j(t) dt = \begin{cases} 0, & i \neq j; \\ p_i, & i = j \end{cases} \quad (i, j = \overline{0, N}), \quad (3)$$

where p_i – signal energy γ_i .

Equation (3) allows for correlation reception and detection of noise signals. However, for such reception it is necessary to have copies of all transmitted signals on the receiver side, which is practically impossible when using real noise generators.

3 Ortho-noise transmitter

Transmitter output signal (transmitting data) $\rho_i \in \{-1, 1\}$ ($i = \overline{1, N}$) form in accordance with the following recurrent equation:

$$\begin{cases} \rho_0 = 1; \\ \rho_i = 0, \end{cases} \quad \gamma_{i+1} = \chi_i + \rho_i \times \frac{(\gamma_i, \chi_i)}{(\gamma_i, \gamma_i)} \gamma_i \quad (i = \overline{0, N}), \quad (4)$$

where γ_i – i -th output noise pulse of the transmitter, χ_i – i -th input noise pulse of the noise generator. The mutual energy of adjacent noise pulses will be equal to (γ_{i+1}, γ_i) ,

$$(\gamma_{i+1}, \gamma_i) = \int_0^T \gamma_{i+1}(t) \times \gamma_i(t) dt = (\chi_i, \gamma_i) + \rho_i \times (\chi_i, \gamma_i). \quad (5)$$

From (5) it follows that when $\rho_i = -1$ noise pulse γ_{i+1} will be orthogonal to the noise pulse γ_i , and when $\rho_i = 1$ – is collinear to it, i.e. The mutual energy of the pulses will either be zeroed or doubled.

The block diagram of an ortho-noise transmitter that implements the formulas is shown in Figure 1, and one of the ortho-noise signal implementations shown in Figure 2.

At the transmitter output, a signal normalization unit can be used, which allows the output signal to be obtained without a noticeable change in instantaneous power caused by orthogonalization or collinearization of noise pulses [6].

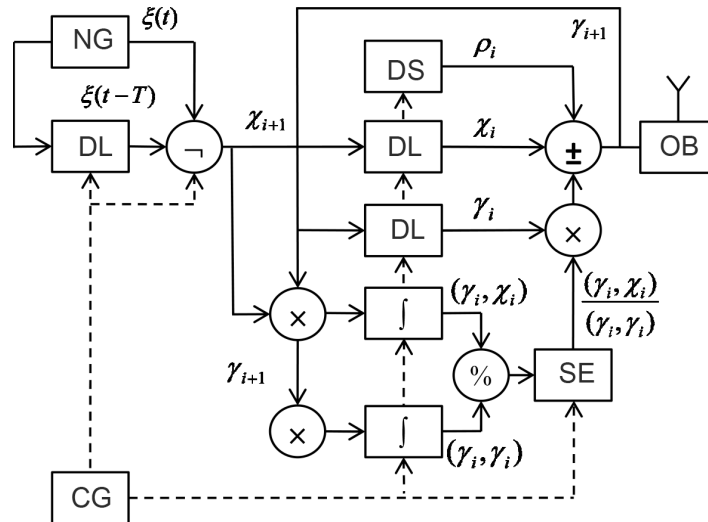


Fig. 1. Ortho-noise transmitter:
 NG – noise generator, CG – clock generator, DS – data source, DL – delay line, SE – storage element, OB – output block, \ominus – inverter, \oplus – adder-subtractor, \times – multiplier, $\%$ – divisor, \int – integrator with reset.

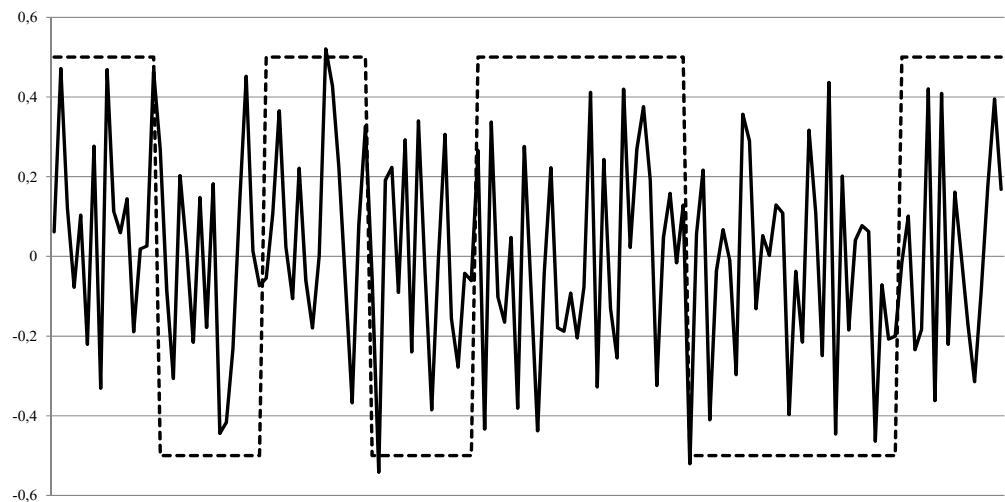


Fig. 2. The ortho-noise signal at the transmitter output during data transmission is 01011001, where the first transmitted noise pulse is starting one.

4 Synchronization signal transmission

A delay line and an inverter are used to synchronize the receiver and transmitter [7] ensuring a sign change of the neighboring noise pulses mutual energy:

$$\chi(t) = \sigma \times \xi(t) \quad (t \in [0, \infty)),$$

where $\xi(t)$ – signal from the noise generator, σ – inverting multiplier, $\chi(t)$ – a synchronized noise signal such that the mutual energy of adjacent pulses changes its sign at each clock interval (Fig. 3):

$$\sigma = \begin{cases} -\tau, & \xi(t) \times \xi(t-T) < 0; \\ +\tau, & \xi(t) \times \xi(t-T) \geq 0, \end{cases} \quad \tau = \begin{cases} -1, & t \in [2nT, (2n+1)T); \\ +1, & t \in [(2n+1)T, 2nT), \end{cases} \quad n = 0, 1, 2, \dots$$

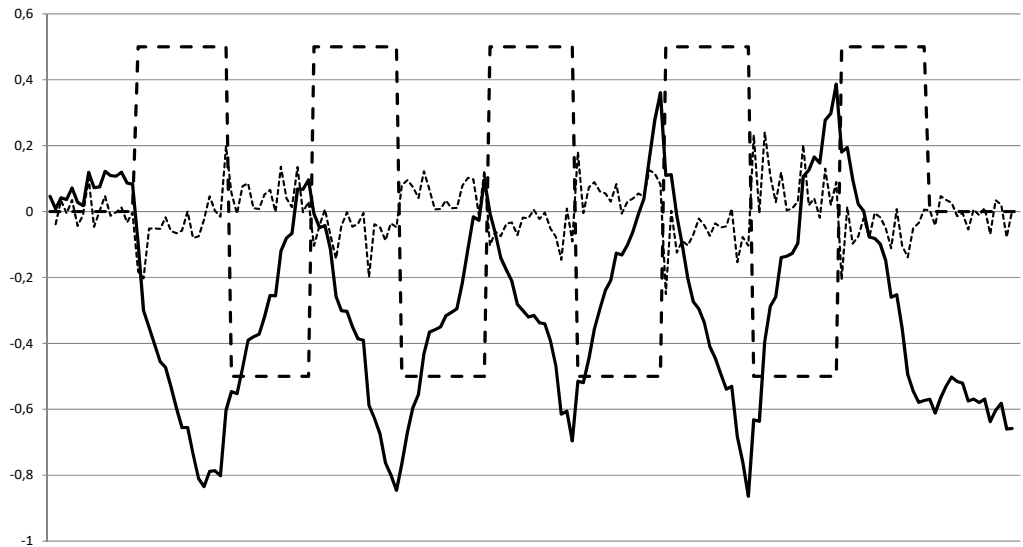


Fig. 3. Integral of the instantaneous mutual energy of the direct and delayed noise signal with noise in the communication channel (solid curve), first derivative of the mutual energy (dashed curve), original clock signal (dashed curve)

5 Ortho-noise receiver

Transmitted data ρ_i on the receiving side are detected as follows:

$$\rho_i = \begin{cases} -1, & |\gamma_i, \gamma_{i+1}| < \frac{\varepsilon}{2} \times (\gamma_i, \gamma_i); \\ +1, & |\gamma_i, \gamma_{i+1}| \geq \frac{\varepsilon}{2} \times (\gamma_i, \gamma_i), \end{cases} \quad t_i: \frac{d}{dt} \left(\int_0^{T+\Delta T} \gamma_i(t) \times \gamma_{i+1}(t) dt \right) = \pm \Delta \quad (i = \overline{1, N}), \quad (6)$$

where γ_{i+1} (γ_i) – current (previous) noise pulse, t_i – impulse end moment γ_i , ΔT – maximum synchronization error, Δ – clock signal threshold, ε – minimum value of the relative mutual energy modulus of the noise generator adjacent noise pulses,

$$\varepsilon = \min_{i=0}^N \frac{|(\chi_i, \chi_{i+1})|}{(\chi_i, \chi_i)}.$$

The block diagram of an ortho-noise receiver that implements formulas (6) is shown in Figure 4.

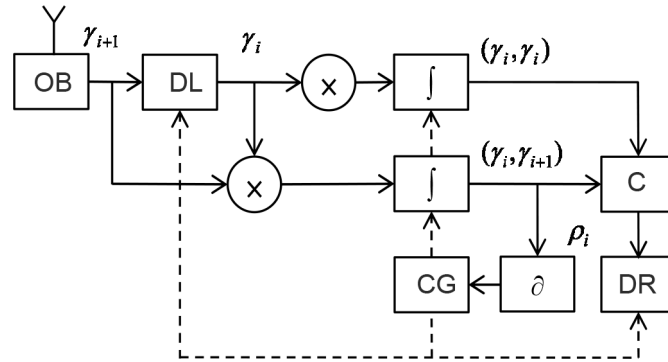


Fig. 4. Ortho-noise receiver: RIB – receiver input block, ISDL – input signal delay line, CG – clock generator, C – comparator, DR – data receiver, \times – multiplier, \int – integrator with reset, ∂ – low pass filter and differentiator

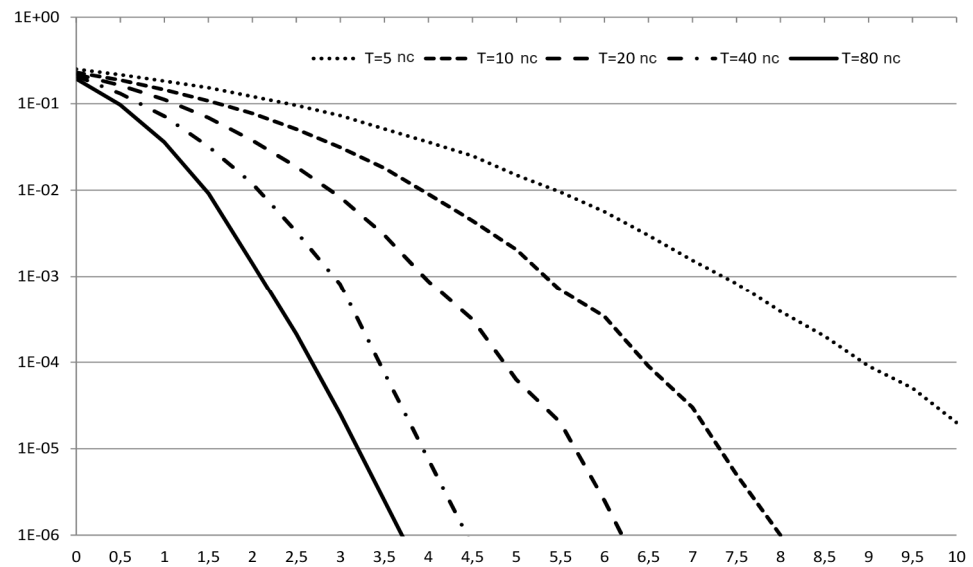


Fig. 5. Dependence of the erroneous reception probability of one bit of data on the signal energy ratio to spectral noise density in the 2.1 GHz frequency band (dB)

6 Conclusion

Good correlation, spectral and statistical properties of noise signals will allow them to be effectively used in advanced communications. The results of an experimental test of the noise immunity of ortho-noise data transmission are shown in Figure 5. The graph shows that for a given signal-to-noise ratio, by increasing the duration of the noise pulses, an arbitrarily small probability of erroneous reception of one bit of data can be achieved. It should be noted that the transformations of the original noise signals used in the transmitter do not significantly affect the correlation, spectral and statistical characteristics of the noise source.

To increase transmission secrecy, you can use normalization of transmitted noise pulses, as well as random or pre-agreed changes in the duration of noise pulses and the phase of the synchronization signal. There are also no obstacles to using a chaotic signal generator instead of a master noise generator.

REFERENCES

- [1] M. Ji, J. Chen and L. Lv, "Non-Orthogonal Multiple Access With Signal Alignment in Two-Way Relay System," *2021 13th International Conference on Wireless Communications and Signal Processing (WCSP)*, Changsha, China, 2021, pp. 1-5, doi: 10.1109/WCSP52459.2021.9613626.
- [2] S. Vakalis and J. A. Nanzer, "Analysis of Element Failures in Active Incoherent Microwave Imaging Arrays Using Noise Signals," *IEEE Microwave and Wireless Components Letters*, vol. 29, no. 2, pp. 161-163, Feb. 2019, doi: 10.1109/LMWC.2018.2890246.
- [3] J. Chen, L. Zhao, C. Li and Z. Niu, "Design of Clock Synchronization based on Wireless Clock Difference Negative Feedback for Independent Distributed Pseudolite Systems," *2022 IEEE 6th Advanced Information Technology, Electronic and Automation Control Conference (IAEAC)*, Beijing, China, 2022, pp. 1456-1460, doi: 10.1109/IAEAC54830.2022.9929594.
- [4] W. Song et al., "A 16-Channel Neural Recorder with 2.8 nJ/bit, 971.4 kbps sub-2.4 GHz polar transmitter," *2022 IEEE International Symposium on Circuits and Systems (ISCAS)*, Austin, TX, USA, 2022, pp. 2710-2714, doi: 10.1109/ISCAS48785.2022.9937786
- [5] G. Huang, D. Zhang, W. Chen and Y. Chen, "Accelerated Signal-and-Noise Orthogonalization," *IEEE Transactions on Geoscience and Remote Sensing*, vol. 60, pp. 1-9, 2022, Art no. 5901909, doi: 10.1109/TGRS.2021.3054839.
- [6] K. -F. Un, F. Zhang, P. -I. Mak, R. P. Martins, A. Zhu and R. B. Staszewski, "Design Considerations of the Interpolative Digital Transmitter for Quantization Noise and Replicas Rejection," *IEEE Transactions on Circuits and Systems II: Express Briefs*, vol. 67, no. 1, pp. 37-41, Jan. 2020, doi: 10.1109/TCSII.2019.2903561.
- [7] K. Matsuura, K. Shin, D. Kobuchi, Y. Narusue and H. Morikawa, "Synchronization Strategy for Distributed Wireless Power Transfer With Periodic Frequency and Phase Synchronization," *IEEE Communications Letters*, vol. 27, no. 1, pp. 391-395, Jan. 2023, doi: 10.1109/LCOMM.2022.3212692.
- [8] K. Lukin, O. Zemlyanyi and S. Lukin, "Generation of Chaotic and Random Signals for Noise Radar – Brief Overview," *2022 23rd International Radar Symposium (IRS)*, Gdansk, Poland, 2022, pp. 163-168, doi: 10.23919/IRS54158.2022.9905030.